University of Nevada, Reno

Phenology-based UAV remote sensing for classifying invasive annual grasses to the species level

A thesis submitted in partial fulfillment of the
requirements for the degree of Master of Science in
Natural Resources and Environmental Science

by

Alice A. Ready

Peter J. Weisberg / Thesis Advisor

August, 2021

THE GRADUATE SCHOOL

We recommend that the thesis
prepared under our supervision by

entitled

be accepted in partial fulfillment of the
requirements for the degree of

Advisor

Committee Member

Graduate School Representative

David W. Zeh, Ph.D., Dean
Graduate School

PREAMBLE

The research presented in this thesis is written with the intention of future publication in a peer-reviewed scientific journal. I will be the primary author on the paper, with Peter Weisberg as second author, and Tom Dilts and Chris Kratt as subsequent co-authors. Hence, I use pronouns in the plural rather than the singular throughout this thesis.

ABSTRACT

The spread of invasive plant species severely alters wildfire regimes, degrades critical habitat for native species, and has detrimental impacts on ecosystem function, rangeland productivity, and long-term carbon storage dynamics. Remote sensing technology has greatly improved our understanding of invasive plant ecology and ability to map and monitor plant invasions. Mapping plant invasions to the species level with conventional satellite and airborne data has proven challenging, however, because many invasive species occur at fine spatial scales or are mixed with native species, and satellite passes may occur too infrequently to capture important phenological stages. Imagery derived from readily deployable Unmanned Aerial Vehicles (UAVs) offers high-resolution data over carefully timed acquisition dates during the growing season. However, some challenges remain that are particular to high spatial resolution imagery, where excessive detail from shadows and canopy gaps often result in misclassification, inaccuracy, and a "salt-and-pepper" effect in the final classification. The addition of textural and vegetation height data to a purely spectral pixel-based approach has the potential to mitigate these challenges and improve species-level vegetation classification. Using UAV imagery

acquired at specific phenological stages, we investigate which combinations of spectral, textural, vegetation height, and multi-temporal techniques best separate two invasive annual grasses, cheatgrass and medusahead, to the species level.

We selected five study sites ranging in area from 8 to 36 hectares (ha) in Paradise Valley, Nevada, which feature a variety of invasive and native species that are typical of the Great Basin region. For three carefully selected dates over the growing season during which cheatgrass and medusahead were most spectrally distinct, we conducted UAV flight campaigns and collected field data on vegetation composition. Imagery was processed in photogrammetric software to produce orthomosaics, digital terrain models, and digital surface models from which vegetation height was derived. Texture analysis was performed over the acquired raster data products. Multi-date spectral, textural, and vegetation height variables were used to predict vegetation class type using Random Forest machine learning methods.

The overall goal of this research is to further remote sensing methods for vegetation classification of invaded landscapes to the species level. We investigated which combinations of spectral, textural, vegetation height, and multitemporal techniques best separate two invasive annual grasses - cheatgrass and medusahead. To explore the impact of explanatory variables in our classification, all possible additive combinations of our variables were calculated. We found that multi-temporal texture variables and vegetation height added additional levels of information to our classification and, when combined

with multi date spectral information, achieved the highest overall accuracy. Our model resulted in a robust classification across several diverse study sites.

ACKNOWLEDGMENTS

Foremost, I would like to express my sincere gratitude to my advisor and committee chair, Peter Weisberg, for giving me the opportunity to pursue research and providing invaluable guidance over the course of my graduate career. His expertise and insight truly made this thesis beyond my highest expectations. Peter not only challenged and inspired me to grow professionally as a scientist but also as a person. I am proud of, and grateful for, my time working with Peter.

In addition to my advisor, I would like to thank my thesis committee, Jonathan Greenberg and Kenneth Nussear, for their thoughtful comments, rigorous coursework, and timely feedback. I would also like to offer special thanks to Thomas Dilts for generously offering his time and expertise over the past two years. He was always eager to assist with my remote sensing and modeling questions, big or small, and warmly welcomed me into the Great Basin Landscape Ecology Lab (even in 100-degree fieldwork!). My appreciation extends to my colleagues in the Great Basin Landscape Ecology Lab, Paul Burow, Israel Borokini, Charlene Duncan, Natasha Wesely, and Georgia Vasey for the endless support, practice talks, feedback, and positive atmosphere in which to do science. And during most uncertain times, I would not have been able to proceed with a socially distanced field season were it not for everyone's willingness to volunteer their time and efforts.

This research was funded by the Nevada Department of Wildlife (Habitat Conservation Fee Special Reserve Account) in a cooperative agreement with the USDA Forest Service

Humboldt-Toiyabe National Forest (federal award 17-GN-11041730-25) and the Nevada Space Grant Consortium (National Aeronautics and Space Administration Grant No. 80NSSC20M0043). Support was also provided by the University of Nevada, Reno, Graduate Student Association. Contents of this thesis are solely the responsibility of the authors and do not necessarily represent the official views of the Nevada Department of Wildlife. Thank you to project collaborators: Bobby Smith with Nevada Department of Wildlife and Monique Nelson, Meagan Carter, Boyd Hatch, and Dirk Netz with Humboldt-Toiyabe National Forest. UAV data collection and image processing were supported by the Centers for Transformative Environmental Monitoring Programs (CTEMPs) under National Science Foundation Awards EAR 1440506. Thank you to Scott Tyler for providing support and infrastructure for this project. Special thanks to Christopher Kratt for his knowledge regarding UAV flights, protocol, and photogrammetry which contributed to much of the UAV data used in this project.

Last but not the least, I am forever grateful for the support and encouragement of my family. Dad, thank you for fielding numerous phone calls, proofreading anytime, and inspiring me to pursue the endeavors of my passion and higher education. Thank you to my sister, Margaret, for never failing to make me laugh when I needed it most and always reminding me of what's important. And I am most indebted to Grandmother Arlene, whose farm work, fishing trips, and knowledge of the land inadvertently inspired me to pursue my interests in science by sparking a boundless curiosity and appreciation for the natural world.

TABLE OF CONTENTS

LIST OF TABLES

LIST OF FIGURES

Distinguishing invasive annual grasses to the species level, using phenology-based spectral, textural, and structural data derived from Unmanned Aerial Vehicle imagery

ABSTRACT

We capitalized on species-specific differences in plant phenology and use high-resolution Unmanned Aerial Vehicle (UAV) imagery to classify invasive annual grasses (cheatgrass (*Bromus tectorum*) and medusahead (*Taeniatherum caput-medusae*) to the species level and distinguished them from native rangeland species. UAVs can produce images at the centimeter scale, largely avoiding the 'mixed-pixel problem' where larger pixels encompass multiple cover types and plant species. However, purely pixel-based approaches at high spatial resolutions often result in misclassification due to excessive detail arising from plant structural features like leaf angle, canopy gaps, or shadows. Our study addressed this challenge by employing a novel combination of spectral, textural, vegetation height, and multitemporal phenology-based data in a Random Forest classification. Exploratory data analysis illustrated unique patterns in the distributions of spectral, textural, and vegetation height data for each vegetation class type. After iterating through all possible model combinations of our variables, we found that the top six best performing models utilized texture and height variables in addition to phenology-based spectral data. Our approach proved generalizable across multiple large rangeland sites and distinguished invasive plant species from one another and from the dominant species of native vegetation within which they are embedded, increasing the utility of remote sensing data in invasive species management. Scaling our classification to regional or

continental levels and incorporating historical imagery would allow for risk assessments of future invasion and further our knowledge of invaded plant communities.

KEYWORDS: invasive species, cheatgrass, *Bromus tectorum,* medusahead, *Taeniatherum caput-medusae,* weed detection, texture analysis, UAV, phenology

INTRODUCTION

Invasive annual plants are transforming arid and semiarid ecosystems into low-diversity, wildfire-prone, and economically unproductive grassland monocultures (Abatzoglou and Kolden 2011; Heywood, 1989; Mack et al., 2000; Walker and Steffen, 1997). With climate change and large-scale disturbances accelerating the spread of invasive annual grasses, the efficient control of emerging infestations is critical for slowing the rate of invasion and promoting rangeland biodiversity in regions that are potentially at risk (Archer and Predick 2008; Davies and Johnson 2008). Efforts to control the expansion of invasive plants are, however, limited by imperfect knowledge of spatial distribution. Traditional field-based surveys can collect detailed and accurate data regarding the spatial distribution, population size, and trends of plant communities (Sutherland, 2006), however, field surveys are generally limited to small, sampled areas and specific field seasons (Kerr and Ostrovsky, 2003). Often used in accordance with field-based data, remotely sensed data has been widely used in mapping and monitoring the distribution and abundance of invasive plant species (Bradley, 2014; Huang and Asner, 2009; Joshi et al., 2004). For targeted weed control applications, understanding patterns of species composition and diversity at the *species level* is essential for site-specific weed mapping

and the early detection of new invasions (Marushia et al., 2010). To address the existing limitations of high spatial resolution imagery and develop generalizable classifications of invasive annual plants to the species level, we combine phenology-based spectral, textural, and vegetation height information within a Random Forest classification framework. This additional representation of landscape characteristics builds upon and extends previous studies which exclusively use spectral attributes to classify invasive plants (de Sá et al., 2018; Doody et al., 2014; Weisberg et al., 2021).

Like much of the Western United States, the once diverse Great Basin ecosystems are rapidly converting to winter annual grasslands containing prevalent exotic species such as cheatgrass (*Bromus tectorum*), medusahead rye (*Taeniatherum caput-medusae*), and wiregrass (*Ventenata dubia*) (Davies and Johnson, 2008; Hironaka, 1994; Tortorelli et al., 2020). With the introduction of exotic annual grasses and domestic livestock from Eurasia, native perennial grasses were overgrazed and replaced by winter annual grasses over the last 200 years (Young and Longland 1996). Non-native grasses continue to expand into shrubland ecosystems, causing rapid conversion into annual grasslands and consequently altering fuel load, critical habitat for native species, ecosystem functions, rangeland productivity, and dynamics of long-term carbon storage (D'Antonio and Vitousek 1992; Brooks et al., 2004; Bradley et al., 2006). This results in dense monocultures that can reestablish more quickly than native species after a fire event, ratcheting up the dominance of invasive grasses following each successive disturbance (D'Antonio and Vitousek 1992; Melgoza et al., 1990).

Our study focuses on two invasive grass species of significant concern for management and conservation: cheatgrass and medusahead. These highly competitive species spread over short distances by wind and water, while at large distances they are effectively dispersed by attaching to animals, humans, and machinery (Davies and Sheley, 2007; Hulbert, 1955). While cheatgrass is a well-established invader in the Great Basin region, the rapid spread of medusahead has been more recent (Nafus and Davies, 2014; Young 1992). Thus, development of new remote sensing approaches for early and species-specific detection of cheatgrass and medusahead invasions will be timely and advantageous for allowing range managers to control their further spread.

Historically, species-specific mapping has been limited by the relatively low spatial and temporal resolutions of aerial and satellite imagery platforms, which are too coarse to identify isolated individuals or small patches of invasives and unable to differentiate spectrally similar vegetation types (Carson et al., 1995; Lawrence et al., 2006). Several studies have successfully mapped invasive plants to the species level by employing phenology-based multitemporal imagery for classification (Carson et al., 1995; Everitt et al., 1992; Peterson, 2005; Schriever and Congalton, 1995; Singh et al., 2018). Species-specific differences in phenology provide an opportunity to distinguish invasive species from one another and the ecosystem in which they are embedded. The phenology of a plant during the growing season, including life-cycle events such as emergence, flowering, or senescence, emphasizes the spectral differences between vegetative types (Justice et al., 1985; Reed et al., 1994). For example, saltcedar (*Tamarix spp*.) invasions were effectively mapped using images from late fall when foliage is a distinct orange-

yellow color as opposed to other riparian species (Ji and Wang, 2016). Species can be separated based on varied phenological stages within the same image, or when phenology differs between images (Singh et al., 2018).

Invasive annual grasses such as cheatgrass have been classified using intra-annual spectral differences between active and senescent periods (Boyte et al., 2019; Peterson, 2005), or by using plant-specific responses to inter-annual variability in precipitation (Balch et al., 2013; Bradley and Mustard, 2005; Bradley and Mustard, 2006). While these approaches are successful at identifying invasion patterns at regional scales, multiple species of similar phenology are consequently grouped together and do not generate the species-specific classifications required for more targeted management.

Although our two species of interest are similar in structure and stature, identification to species is possible because the phenological attributes of each are distinctive from one another and from native vegetation (Figure 1). Cheatgrass reaches peak greenness early in the season, develops a reddish seedhead, and becomes senescent in late spring when native species are still green (Figure 1A, 1B, and 1C) (Peterson, 2005). While other annual grasses are brown, medusahead turns a bright yellow-green color in spring and early summer. As the plant matures over the growing season, it stays green longer than cheatgrass and other forbs (Figure 1D and 1E). Nearing senescence, medusahead becomes a pale-yellow color and eventually tan (Figure 1F) (Ndzeidze, 2011).

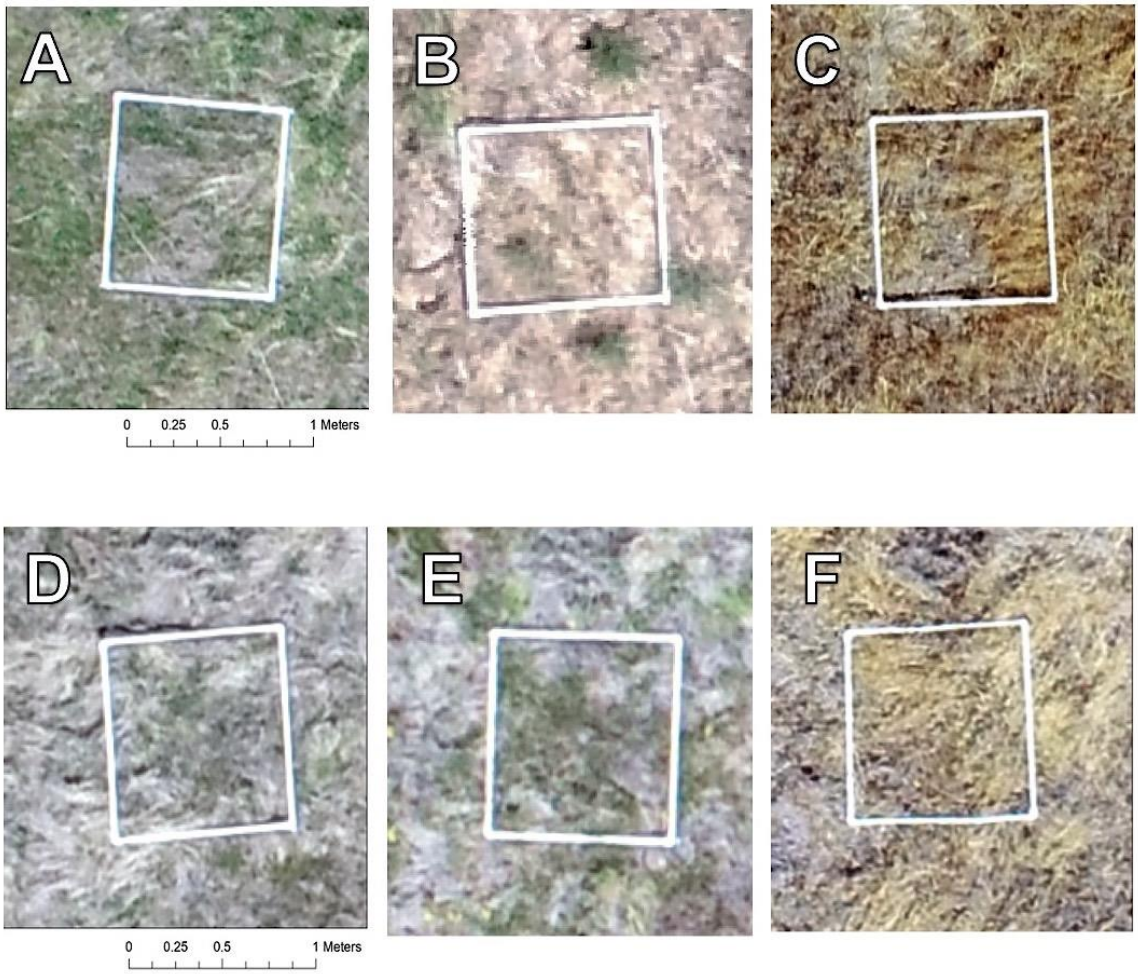

Figure 1. UAV imagery emphasizing differences in plant phenology for cheatgrass and medusahead. Panels show quadrat frames for (A) cheatgrass mid-May; (B) cheatgrass early June; (C) cheatgrass early August; (D) medusahead mid-May; (E) medusahead early June; (F) medusahead early August.

In 2017, Weisberg and co-authors used multitemporal UAV imagery to distinguish multiple co-occurring species of invasive annual grasses from each other and from native Intermountain West vegetation, based on phenological differences in the timing of plant life phases over the course of a growing season. By oversampling eight different dates of UAV imagery, a species-specific classification was best optimized using three flight dates: May 19th, June 1st, and July 20th (Weisberg et al., 2021). This three-date model

resulted in high classification accuracies for cheatgrass and medusahead and reasonable overall accuracy, considering the high number of class types (a total of 9 class types) (Weisberg et al., 2021).

While phenology has proven successful in separating cheatgrass and medusahead in a pixel-based classification (Weisberg et al., 2021), challenges remain with the use of high spatial resolution imagery, such as UAV imagery. Pixel-based landcover classifications at high spatial resolutions frequently contain excessive spatial detail caused by variations in features such as leaf angle, shadows, and canopy gaps, often resulting in misclassification arising from a "salt-and-pepper" effect (de Jong et al., 2001; Kelly et al., 2004; Van de Voorde et al., 2007). There has been success in overcoming this challenge by using texture, object-oriented, or spatialized classification which use a pixel's neighborhood characteristics in addition to its spectral characteristics (Blaschke et al., 2000; Dell'Acqua and Gamba, 2006; Yoon et al., 2005). While spectral features provide the average tonal variation in various bands of the electromagnetic spectrum, textural features provide information about the spatial distribution of tonal variations across pixels within a single band (Haralick et al., 1973). Such textural information obtained within the spatial neighborhood of a pixel provides additional information regarding distinct spatial structures that can be linked to specific vegetation types (Coburn and Roberts, 2004; Ge et al., 2006; Riou and Seyler, 1997).

A wide variety of approaches exist to describe landscape texture, but perhaps the most widely used technique involves gray-level occurrence and co-occurrence metrics within a

moving window, or kernel (Haralick and Shanmugam, 1974; Haralick et al., 1973). First-order texture statistics summarize the counts, or occurrences, of pixel values within the moving kernel of a designated window size (Unser, 1986). Second-order texture metrics, also referred to as co-occurrence measures, incorporate the relationship between neighboring pixels. Smooth textures are characterized by within-feature variability that is lower than between-feature variability, whereas for coarse textures, the converse is true (Ferro and Warner 2002; Haralick et al., 1973). This characteristic of texture is favorable when separating relatively smooth surfaces in an image (water or bare ground) from coarser surfaces (urban or vegetated areas) (Laliberte and Rango 2009). At detailed resolutions, texture can be used to differentiate patches of grass from shrubs, which have coarser texture due to shadows, branches, and twigs juxtaposed with foliage (Laliberte and Rango 2009). Classification accuracy is often improved with inclusion of texture, particularly for high-resolution data such as UAV imagery (Feng et al., 2015).

Plant species differ in height, making variation in vegetation height another key expression of plant structure. Several studies have reported an increase in overall classification accuracy with the inclusion of structure and height data, particularly in heterogeneous landscapes, as opposed to using only spectral variables (Räsänen and Virtanen, 2019; Rosso et al., 2006; Straatsma and Baptist, 2008). In fact, detailed vegetation height information can readily be calculated from aerial imagery flown with sufficient overlap using photogrammetric techniques (e.g. structure-from-motion; Westoby et al., 2012). Orthomosaic and height models derived from 3-dimensional UAV data have been reported to accurately classify vegetation using image segmentation and

decision trees (Fraser et al., 2016; van Iersel et al., 2018). In the low-Arctic, Fraser et al. (2016) calculated vegetation heights at the 1cm scale using structure-from-motion methods in the monitoring of short-statured tundra vegetation. This additional information derived from UAV imagery can be utilized in classifications capturing fine-scale heterogeneity of vegetation at local scales.

By capitalizing on differences in plant phenology and the ability of Unmanned Aerial Vehicles (UAVs) to capture detailed imagery inexpensively and reliably over multiple, frequent, user-defined time periods, we have previously been able to differentiate individual species of invasive annual grasses (medusahead rye vs. cheatgrass) that co-occur over much of the western United States (Weisberg et al., 2021). Our objective is to refine this multi-temporal methodology by incorporating additional levels of vegetation complexity beyond phenology, with the addition of texture and vegetation height (Figure 2). We further extend the approach to a larger and more heterogeneous study area, leading to a more generalizable assessment and technique. Our analysis investigates three main questions (1) How does our methodology perform for larger, more numerous, and more diverse landscapes? (2) Which combinations of spectral, textural, vegetation height, and multitemporal information sources best distinguish two invasive annual grasses, cheatgrass and medusahead, to the species level? (3) Which variables contribute the most to classification performance?

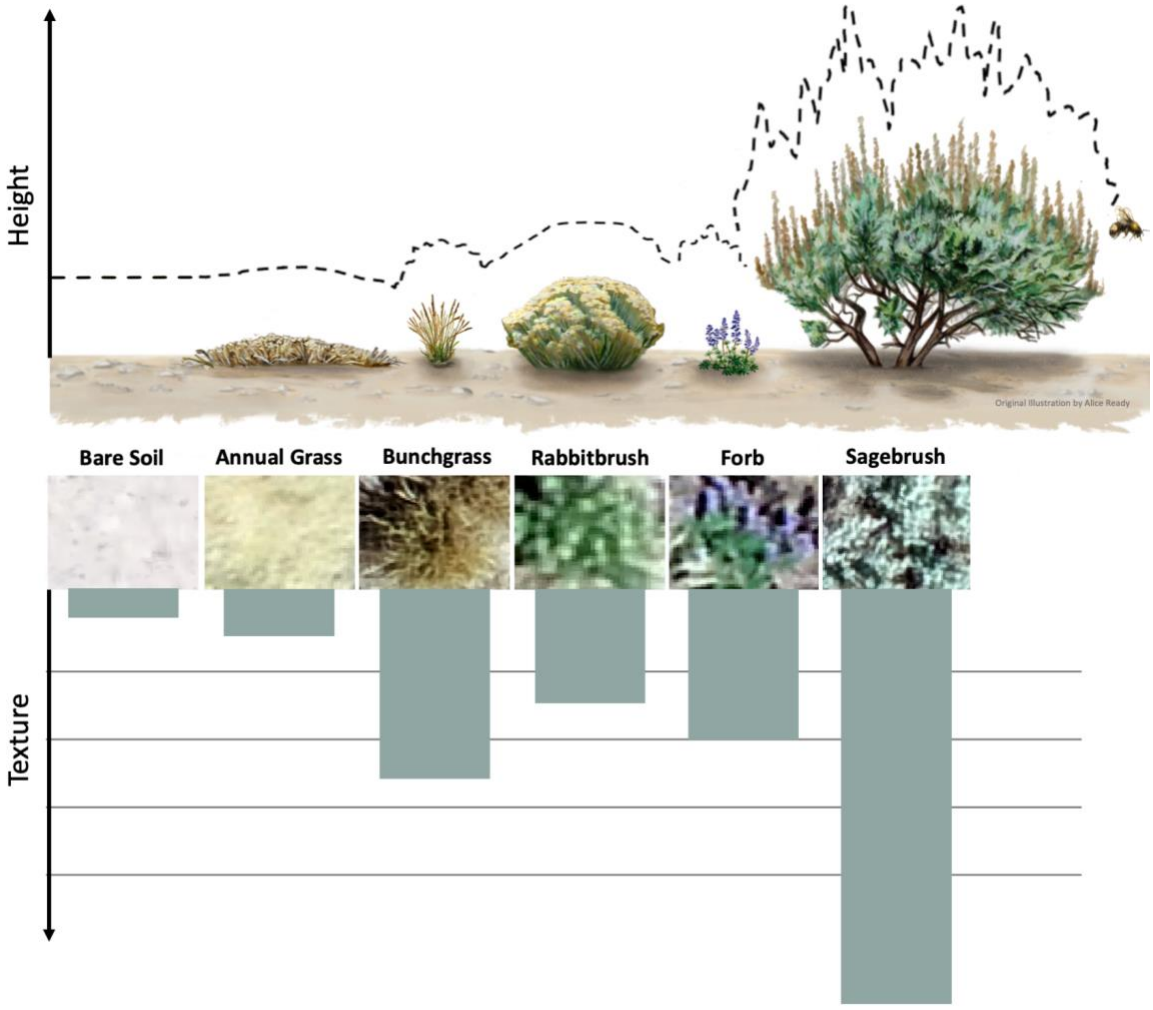

Figure 2. A conceptual illustration of texture and height for class types which are representative of a sagebrush steppe ecosystem, ranging from bare soil to sagebrush. The dotted line represents the theoretical path of a bumblebee as it maintains a constant elevation above the upper surface of vegetation. The flatness of the bee's dotted line represents low texture, while irregularity in the dotted line represents high texture. Samples of imagery illustrate the variability in pixel values within the moving kernel window for each vegetation type. The downward-facing column graph demonstrates relative texture values between vegetation types, irrespective of vegetation height. Bare soil and annual grasses have low texture values, while bunchgrass and sagebrush are characterized by high texture.

METHODS

Our methodological processes can be broken down into five core steps: data collection, image processing, extracting variables, image classification, and accuracy analysis (Figure 3). The first step, data collection, involves all field-based acquisitions of vegetation data, UAV imagery, and ground control points. Once UAV imagery is collected, image processing requires the registration, orthorectification, and mosaicking of UAV images to generate raster file data. Because our approach is inherently an iterative process, steps one and two are repeated in June and August before the extraction of variables in step three. After all dates of imagery are processed, pure patches of vegetation are photo-interpreted, texture analysis is performed, vegetation height is calculated, and RGB spectral data is extracted in step three. In step four of image classification, Random Forest (RF) is applied to the response variable (photo-interpreted vegetation class type) and predictor variables (phenology-based spectra, texture, and vegetation height). Finally in step five, accuracy analysis is performed by predicting the model to validation data of vegetation data collected in the field. Depending on model performance, explanatory variables are refined to generate the most predictive model. Once the top model is determined, classification maps are aggregated to a coarser resolution for the final classification map.

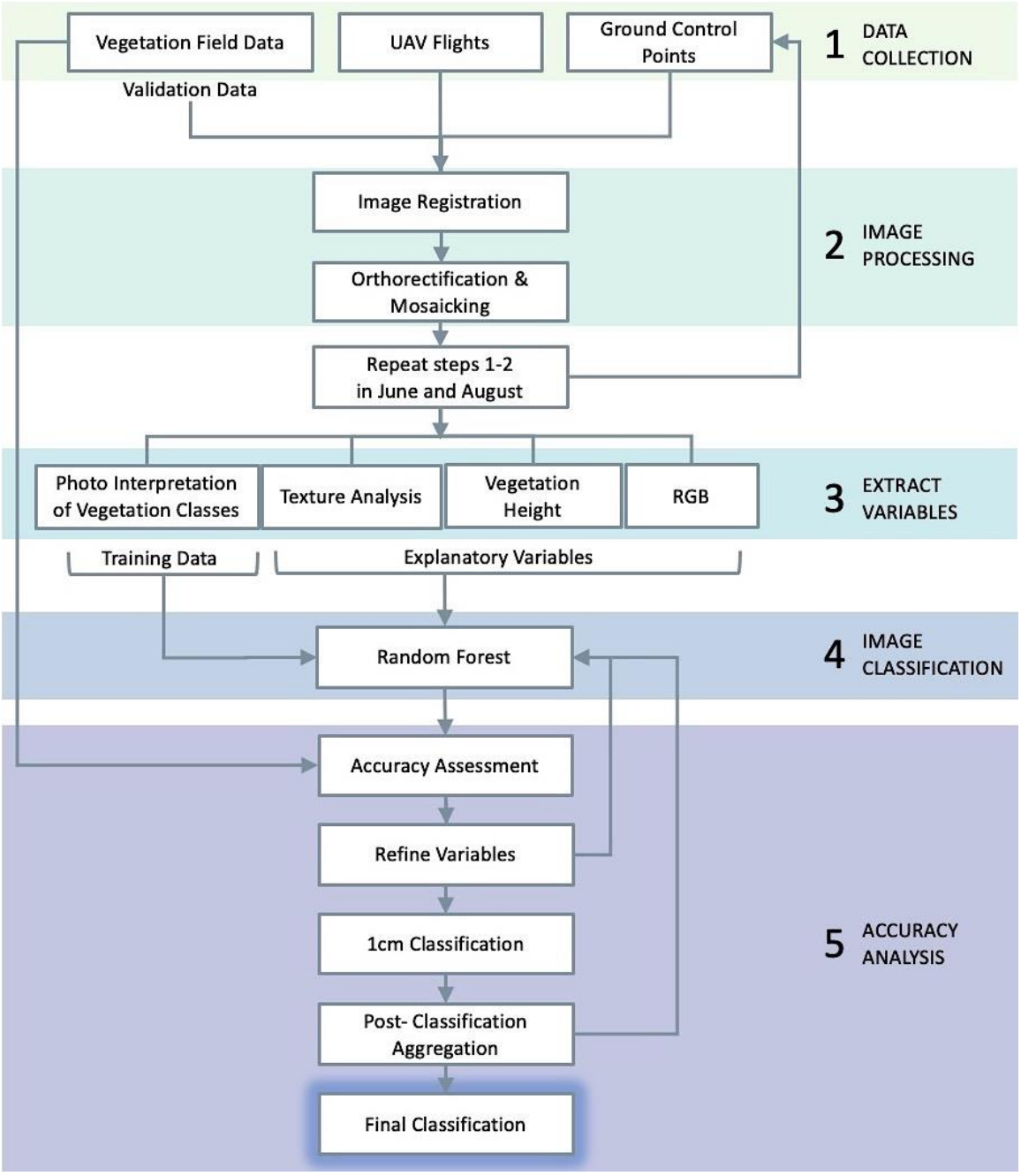

Figure 3. Flow chart of methodology illustrating the overall processes for classifying invasive annual grasses to the species level. Numbered segments from 1 to 5 represent the order in which steps are performed.

Study Area and Site Selection

The study system of Paradise Valley, Nevada provided an excellent test case for our methodological comparisons because it features multiple invasive species of concern to land managers, as well as a diversity of plant community types that are representative of the Great Basin (Table 1). The study was conducted during the summer of 2019 within five separate study sites, ranging from 8 – 36 hectares (37 – 109 acres) in area and elevations ranging from 4787 – 5430 meters. All five study sites total to 94 hectares, encompassed by a larger area of approximately 3300 hectares (Figure 4). The region is characterized as the Upper Lahontan Basin, Semiarid Uplands, and High Lava Plains ecoregions (Griffith et al., 2016). The heterogeneous vegetation communities are dominated by various native and introduced bunchgrasses, Wyoming big sagebrush (*Artemisia tridentata* ssp. *wyomingensis*), bulbous bluegrass (*Poa bulbosa*), antelope bitterbrush (*Purshia tridentata*), rubber rabbitbrush (*Ericameria nauseosa*), wild rye (*Leymus cinereus*), tumble mustard (*Sisymbrium altissimum*), Russian thistle (*Kali tragus*), cheatgrass, and medusahead rye. Soil textures within the study area typically include fine sandy loams and clay loams (US Geological Survey, USA; USGS).

Table 1: Environmental data and vegetation descriptions for each of the five study sites. MAP = Mean Annual Precipitation, MAT= Maximum annual temperature.

Site	Area (ha)	MAP (mm)	MAT (°C)	Elevation (m)	Vegetation
PV1	36	315	31.3	4908	• Mixed medusahead in sagebrush understory • Perennial forbs, e.g., lupine • Sagebrush distributed throughout the site
PV2	15	319	31.8	4787	• Large pure monocultures of medusahead on south side of road • Dense cheatgrass in southeast corner of site • Sagebrush and bitterbrush, particularly on north side of road • Great Basin wildrye and Russian thistle
PV3	8	318	31.1	4879	• Large pure monocultures of medusahead • Some cheatgrass near road edges and shrubs • Some bulbous bluegrass and perennial forbs • Sagebrush and bitterbrush shrubs
PV5	23	386	30.1	5430	• Medusahead monocultures throughout, particularly in northern half of the site • Pure cheatgrass monocultures in center and northeast corner of site • Dispersed sagebrush and rabbitbrush shrubs throughout the site • Seeded crested wheatgrass throughout the site • Some tumble mustard, native perennial forbs, and wild rye
PV6	12	317	31.3	5040	• Pure medusahead monocultures, particularly in the southeast quadrant of the site • Cheatgrass monocultures dispersed throughout the site • Increasing number of sagebrush shrubs with distance from road • Crested wheatgrass throughout the site

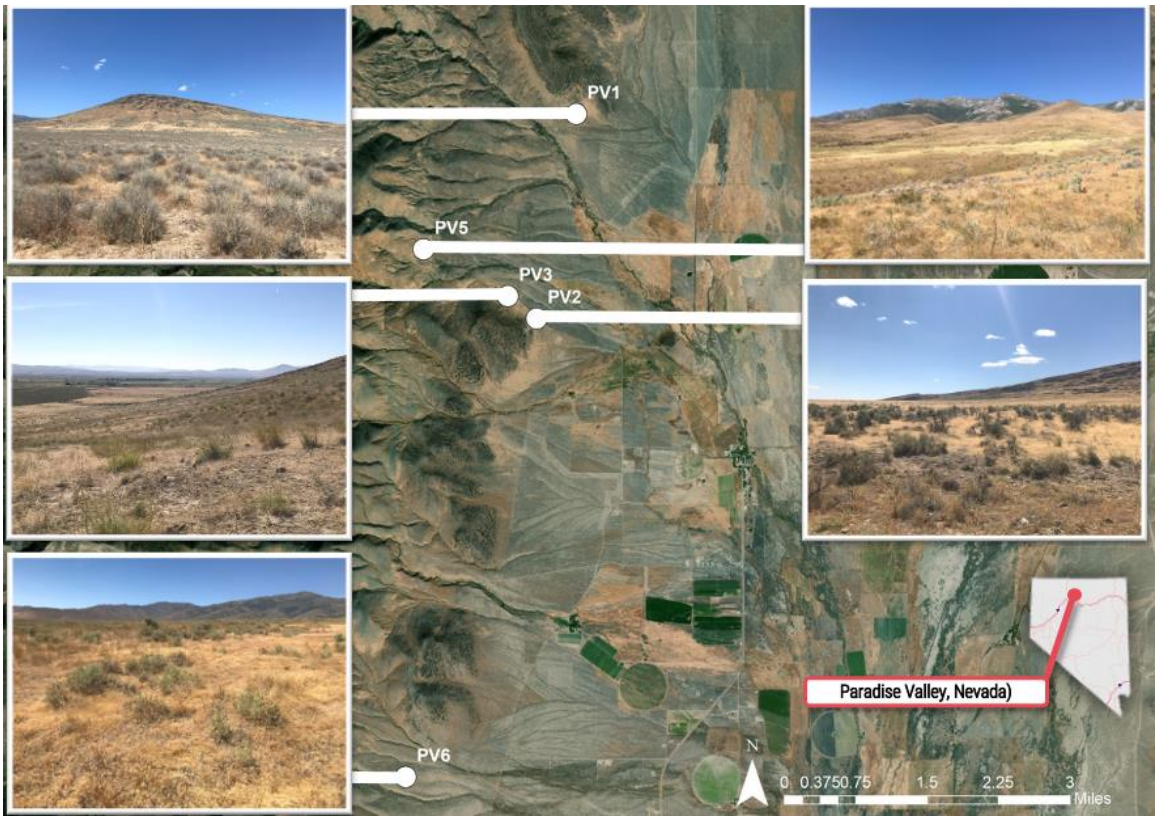

Figure 4. Study sites in Paradise Valley, Nevada, United States. Inset photographs illustrate variations in vegetation between sites (see Table 1).

UAV Flights

UAV data were collected using a Phantom 4 Pro quadcopter (DJI, Shenzhen, Guangdong, China), carrying a true-color RGB camera. The true-color RGB camera is equipped with a one-inch CMOS (complementary metal oxide semiconductor) sensor with ISO values ranging from 100-12,800 and an image resolution of 20 megapixels (5472 x 3078 pixel). This sensor produces visible band spectrum (RGB) true color imagery in RAW file format. A previous study of phenology-based methodology for mapping invasive plant species in the Great Basin found that optimal models using only true-color imagery (i.e. without infra-red bands) require the acquisition of at least three sampling dates over the

growing season (mid-May, early June, and late July/early August) (Weisberg et al., 2021). Therefore, flights were conducted during the following time intervals: May 3 - 5, June 4 - 5, and August 12 – 14. These flight dates were selected to maximize spectral variation between medusahead and cheatgrass arising from differences in their vegetative and reproductive phenology. UAV images were captured mid-day, ± two hours from solar noon to mitigate variability in overall illumination and shadows cast by landscape features. The flight path contained 80% forward overlap and 90% side overlap, to ensure sufficient overlap for successful image mosaicking during processing. Aerial photographs were taken at an altitude of 34 meters above the UAV launch point, resulting in a resolution of one centimeter per pixel, and captured at a speed of five meters per second. Five ground control point (GCP) tiles were placed within each study plot for the duration of the study and verified within drone images to accurately geo-reference images using a Trimble GPS Geo 7x Handheld (Trimble Inc., Sunnyvale, California, USA) with up to 1 cm horizontal and 1.5 cm vertical accuracy.

Collection of Vegetation Data for Model Training and Validation

Two forms of vegetation data were used to develop classification models, including both field data collected from botanical surveys in quadrat frames, and photo-interpreted patches from high-resolution UAV imagery. This approach allowed for model validation that was independent of the data used to develop the vegetation classification. Within pure patches of photo-interpreted vegetation types, points were randomly sampled and used for training data (n = 33,658 points total). We used validation data from two separate sources including field validation data from quadrat frames (n = 4,617 points

total) and sampled points from a randomly selected subset of photo-interpreted polygons across all study sites (n = 16,989 points total).

Field data was collected for 1-m^2 quadrat frames across each of the five study areas (n = 65 quadrat frames total) on the day of each UAV flight. Quadrat frames were placed within areas of relatively homogenous and representative vegetation. Sites PV1 and PV3 did not contain any pure cheatgrass quadrat frames, due to large mixtures of co-existing vegetation. For each one-meter quadrat frame, GPS field measurements were taken using Trimble GPS Geo 7x Handheld (Trimble Inc., Sunnyvale, California, USA) with up to 1 cm horizontal and 1.5 cm vertical accuracy and detailed information regarding plant species and plant functional types were recorded. Within UAV imagery, randomly sampled points were extracted from quadrat frame locations and constrained by a minimum sampling distance of 5 cm. Vegetation data, broadly representative of Great Basin plant communities, was then aggregated to include five different class types: bare soil, bunchgrass, cheatgrass, medusahead, and shrubs.

To obtain training data, pure patches of each vegetation type were manually photo-interpreted from UAV imagery across all study sites (n = 300 polygons total). The average size of photo-interpreted polygons was 0.25m^2 and ranged between 0.01m^2 - 1.07m^2. Photo-interpreted patches were randomly sampled throughout study sites, allowing the proportions of data in each class to be representative of the actual proportions within the study site while capturing different soil types and micro-environments across the entire landscape. Using a minimum sampling distance of 5 cm to

reduce spatial autocorrelation, points were randomly sampled from within photo-interpreted polygons. The proportions of vegetation classes in the training data sample ranged between 10% - 26% (Table 2). To further validate model results after our initial classification, polygons of photo-interpreted vegetation data were randomly selected and partitioned into 50% training and 50% validation data (n = 150 polygons each, training = 16,989 points, validation = 16,669 points). Random selection of photo-interpreted polygons allowed for spatial independence of training versus validation data.

Table 2. Proportions of each vegetation class within training data. Sample points were randomly selected within photo-interpreted polygons.

Class Type	**Percentage of points within the Training Data**	**Sample Size (Points)**
Bare Soil	18 %	6081
Bunchgrass	10 %	3428
Cheatgrass	20 %	6849
Medusahead	26 %	8618
Shrub	26 %	8832

Image Processing

Using raw UAV data collected in the field, overlapping images were processed in Pix4Dmapper Pro software (Pix4D, Switzerland). GCPs were positioned within the UAV point cloud for densification. The differences between known and interpolated locations resulted in an average root mean square error (RMSE) of 2.9cm. Pix4D uses Structure from Motion-Multiview Stereo (SfM-MVS) photogrammetric techniques to tie

overlapping images. The absolute position of the point cloud and matched pixels was reconstructed in a 3D dense point cloud using the X,Y,Z position and spectral information stored for each point. Finally, from the 3D dense point cloud a mesh is interpolated using Inverse Distance Weighting to generate the Digital Surface Model (DSM) and Digital Terrain Model (DTM) rasters at 5cm spatial resolution and orthomosaic rasters at 1cm spatial resolution. Reflectance calibration was not performed during image processing; the lack of calibration is partially mitigated by UAV flights consistently near solar noon and use of band ratios as the spectral predictor variables. To achieve greater spatial alignment of imagery within each site, all orthomosaic, DTM, and DSM rasters were georeferenced into a NAD83 UTM Zone 11 projection using ArcMap (ESRI, USA, CA). Reliable landmarks, such as fence posts, were used in accordance with the coordinate locations of GCP tiles and quadrat frames to georeference orthomosaic images, resulting in an average RMSE of 0.036m.

Phenology-based Spectral Information for Predictor Variables

In addition to performing UAV flights near solar noon, band ratios were calculated using red, green, and blue bands derived from all orthomosaic images to account for spatial and temporal variability in overall illumination. Each spectral band was divided by the sum of all spectral bands (e.g. (Green/(Red + Green + Blue)) to relativize overall illumination on a per-pixel basis. The spectral attributes of band ratios represented the unique phenological characteristics of vegetation class types across May, June, and August imagery in the classification (Table 3).

Table 3. Descriptions of predictor variables used in classification. Phenology-based spectral data is comprised of RGB band ratios. Texture analysis incorporates entropy, skewness, and variance measures. Surface analysis includes vegetation height.

Explanatory Variable	**Imagery Dates**	**Equation**	**Ecological Interpretation**
RGB Band Ratio	May 3 – 5, 2019 June 4 – 5, 2019 August 12 – 14, 2019	*Red / (Red + Green + Blue)* *Green / (Red + Green + Blue)* *Blue / (Red + Green + Blue)*	Band ratios express the unique spectral phenology-based characteristics of vegetation class types over the growing season
Entropy	May 3 – 5, 2019 June 4 – 5, 2019 August 12 – 14, 2019	$Entropy = -\sum_{i=0}^{N_g - 1} P(i) * \ln P(i)$	Entropy isolates complex from less complex variations in vegetation
Skewness	May 3 – 5, 2019 June 4 – 5, 2019 August 12 – 14, 2019	$Skewness = \sum_{i=0}^{N_g - 1} (i - M)^3 P(i)$	Variance highlights abrupt transitions between vegetation patches
Variance	May 3 – 5, 2019 June 4 – 5, 2019 August 12 – 14, 2019	$Variance = \sum_{i=0}^{N_g - 1} (i - M)^2 P(i)$	Skewness enhances edges between vegetation patches while patch interiors contain uniform distributions of points
Vegetation Height	June 4 – 5, 2019	*DSM - DTM*	Vegetation height quantifies variation in plant structure in the Z dimension

Texture Analysis for Predictor Variables

In addition to spectral information from red, green, and blue bands, first-order occurrence measures were used to derive texture metrics that added information on two-dimensional spectral heterogeneity to our classification (Figure 5). The occurrence measure tool in ENVI software (Version 5.0, Harris Geospatial, Broomfield, Colorado, United States) was used over the green band from the orthomosaic image to derive three texture metrics: entropy, skewness, and variance for all dates and sites. The green band was selected for texture analysis because chlorophyll in vegetation absorbs red and blue wavelengths while reflecting green wavelengths, thus best representing the highest signal of vegetation (Curran, 1980; Whittingham, 1974). Texture variables were selected depending on each unique capacity to characterize and highlight variation in species characteristics (Table 3). Entropy, skewness, and variance were calculated using histogram measures based on pixel values within a moving kernel window.

Entropy measures the complexity of pixel values within a moving window by calculating a greyscale diversity index (Shannon, 1948; Wood et al., 2012). The value of entropy increases with spectral heterogeneity, greater evenness, and a greater number of differing greyscale values within the moving window. An orderly kernel window of identical pixel values indicates low entropy (Haralick et al., 1973). Thus, entropy values can isolate complex (sagebrush) from less complex (grass monocultures) variations in vegetation (Figure 5B) (Hall-Beyer 2000).

Boundaries and edges of landscape features are often blurred in aerial imagery. Histogram measures, such as variance and skewness, are commonly used to reduce spectral noise and improve classification accuracy by emphasizing boundaries between features (Kumar et al., 2015). Skewness is calculated as the symmetry or asymmetry from the mean in a normal distribution (Irons and Peterson,1981). Data within a window is symmetrical if skewness equals zero. When skewness deviates from zero in the positive or negative direction, the frequency distribution is more asymmetrical and considered skewed. Edges within the image are enhanced while vegetation patch interiors contain uniform distributions of points (Figure 5C) (Xu et al., 2015).

In a digital image, variance calculates the dispersion of values within the kernel around the mean. First-order occurrence variance differs from traditional variance of grey levels in the original image due to combinations of reference and neighbor cell values used to determine dispersion around the average (Haralick and Shanmugam, 1974; Haralick et al., 1973). Because variance equals zero in areas of equal intensity, boundaries between landscape features are identified in abrupt transitions, resulting in classifications identifying differing class types (Figure 5D) (Kumar et al, 2015). Ground-based vegetation quantification methods commonly use vegetation structure to evaluate habitat variation, making variance an ecologically relevant texture metric (Wood et al., 2012).

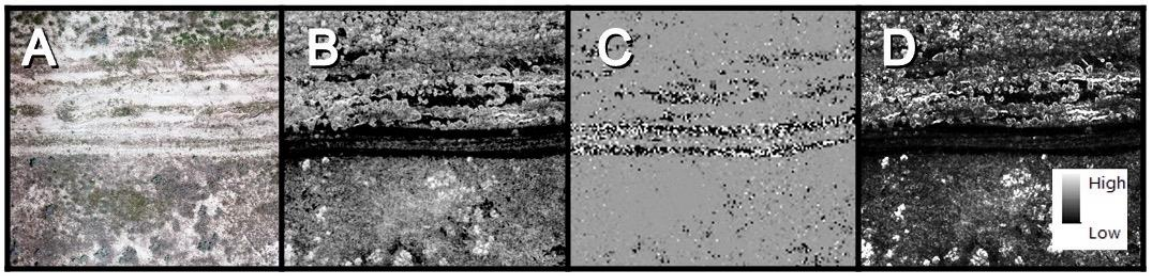

Figure 5. Sample maps illustrating first-order occurrence measures after texture analysis. (A) June orthomosaic for reference. Texture metrics used for predictor variables include (B) entropy, (C) skewness, and (D) variance.

The optimal neighborhood size for calculation of texture metrics has been found to be class-specific (Coburn and Roberts, 2004). At our PV6 site we investigated two window sizes that best encompassed entire shrubs, the largest features for our study region. We found that a window size of fifteen-by-fifteen pixels (Overall = 72%, Kappa = 64%) obtained greater separability between class types than a seven-by-seven window size (Overall = 46%, Kappa = 28%). Accordingly, all texture metrics were calculated using a fifteen-by-fifteen kernel window.

Surface Analysis for Predictor Variables

In addition to the textural measures describing spectral variability or complexity in two-dimensional (2D) space, we also modeled vegetation height to provide 3D information for our classification (Table 3). Digital Surface Models (DSM) are an above-ground measurement of the landscape surface, encompassing natural and artificial features in the environment (Figure 6B). Contrarily, Digital Terrain Models (DTM) are digital representations of underlying ground elevation, removing all natural and built features

(Figure 6C). Using the high-resolution 2D information (X,Y) and altitude (Z value) derived from UAV imagery for each site, vegetation height differences (ΔH) were produced without influence from the underlying topography by subtracting the DTM from the DSM (ΔH = DSM - DTM) (Figure 6D) (Weidner and Förstner, 1995). The DTM and DSM for the June date of imagery were selected because vegetation height for all classes was at peak during this time. The final height variable was transformed to a 1cm resolution to match RGB variables, while retaining original 5cm pixel values.

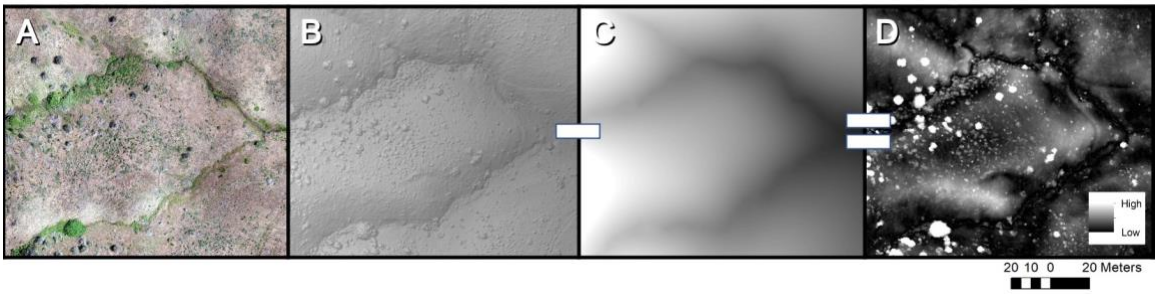

Figure 6. Sample maps illustrating the calculation of vegetation height. (A) June orthomosaic for reference. (B) DSM of above ground landscape features. (C) DTM of underlying ground elevation. The remainder from subtracting the DSM and DTM is (D) vegetation height.

Exploratory Data Analysis of Training Data

Exploratory data analysis (EDA) was used to determine how predictor values distinguish vegetation class types from one another at the species level. Within the photo-interpreted polygons used for training data, EDA illustrated the distributions of predictor variables with each vegetation class type. The minimum, maximum, range, and median values of each explanatory variable was calculated for each vegetation class type. Rather than interpreting red, green, and blue bands individually, we analyzed the more ecologically

relevant green band ratio to visualize overall greenness of spectral data as a surrogate for plant productivity.

Model Classification and Comparison

The Random Forest machine learning method (RF) was used because of its ability to handle complex and high-dimensional remote sensing datasets, such as UAV imagery (Akar and Güngör, 2012; Breiman, 2001; Cutler et al., 2007). RF was applied to the response variable (vegetation class type) and predictor variables (phenology-based spectral, textural, vegetation height characteristics) using R statistical package randomForest (Version 4.6-14; Breiman et al., 2018) to create a classified vegetation map. RF is a nonparametric classification and regression tool which uses a bootstrap method to generate an ensemble of decision trees based on predictor variables, without prior consideration of the response variable (Breiman, 2001). Two hyperparameters, *ntrees* and *mtry*, determine the number of trees in the forest and the number of variables randomly sampled at each split respectively. We found that hyperparameter tuning beyond the default parameters did not significantly affect model performance, and so default values were used where ntrees was set at 1000 and mtry was set to the square root of the number of predictors.

Model predictions were validated using vegetation field data derived from quadrat frames, and then evaluated with classification confusion matrices to compare actual values against predicted values. Training and validation data within individual sites were used to generate single-site models for analyzing the generalizability of a single

classification model containing phenology-based spectral, textural, and vegetation height characteristics. To better understand the unique contribution of each study site and assess the generalizability of a combined site model, five different models were calculated by iteratively excluding each study site while incorporating the remaining four sites.

Next, training and validation data were combined across all five sites to determine the most important combinations of variables in the RF model. Model comparisons were produced by iterating through all possible additive combinations (a total of 31 combinations), without repetition, of all predictor variables. Starting with spectral, textural, and height only models, the unique contributions and synergistic effects of response variables were determined by comparing model improvement with the addition of each variable. Predictor variables for the final classification were selected based on the top performing model using overall accuracy, Cohen's kappa, and balanced accuracy for cheatgrass and medusahead.

To further verify the results of the top performing model, the same 31 combinations of phenology-based spectral, textural, and vegetation height models were applied to training and validation data derived from randomly partitioned polygons of photo-interpreted vegetation data. Results from this classification were compared against the model predictions of the initial model containing both photo-interpreted data for training and quadrat frame data for validation.

Post-classification, the RF model incorporating all five study sites was aggregated using a majority filter. The 1cm resolution of the RF classification contained pixels smaller than vegetative objects of interest, providing excessive detail. Therefore, following RF classification at the 1cm level, multiple scales of aggregation were compared for the classification. After analyzing model fit for multiple window sizes up to a 5cm x 5cm neighborhood, a 2 cm x 2cm majority filter was chosen for the final classification (Supplementary Table 1).

Quantifying the Importance of Predictor Variables

To determine the relative importance of predictor variables in our top model, mean decrease in accuracy (MDA) was calculated as the mean of differences in prediction accuracy between randomly permutated out-of-bag observations (data withheld from the RF model) and the original observations (Cutler et al., 2007). MDA quantified variable importance for class discrimination by calculating loss in model accuracy with the exclusion of each variable. Greater loss in classification accuracy resulted in higher importance for the variable. Variable importance was normalized by dividing the sum of each variable type (spectral, textural, and vegetation height) and the sum of all explanatory variables.

RESULTS

Exploratory Data Analysis of Training Data

Within the photo-interpreted polygons used for training data, distributions of phenology-based spectral, textural, and vegetation height, variables varied consistently across the five vegetation types (Figure 7 and Supplementary Table 2). As expected, bare soil exhibited the lowest median greenness over the entire season (May = 0.329, June = 0.330, August = 0.312; Figure 7A). Bunchgrass generally exhibited the highest median greenness values (May = 0.377, June = 0.378, August = 0.343), with shrubs second (May = 0.343, June = 0.351, August = 0.346). The two invasive annual grass species showed differing temporal progressions of greenness ratio, as expected from species-specific differences in phenology. Median greenness of medusahead increased gradually over the growing season (May = 0.334, June = 0.340, August = 0.342), while median greenness of cheatgrass was higher in May (0.344) but then decreased in June (0.330) during the cheatgrass red phase before senescence in August (0.336).

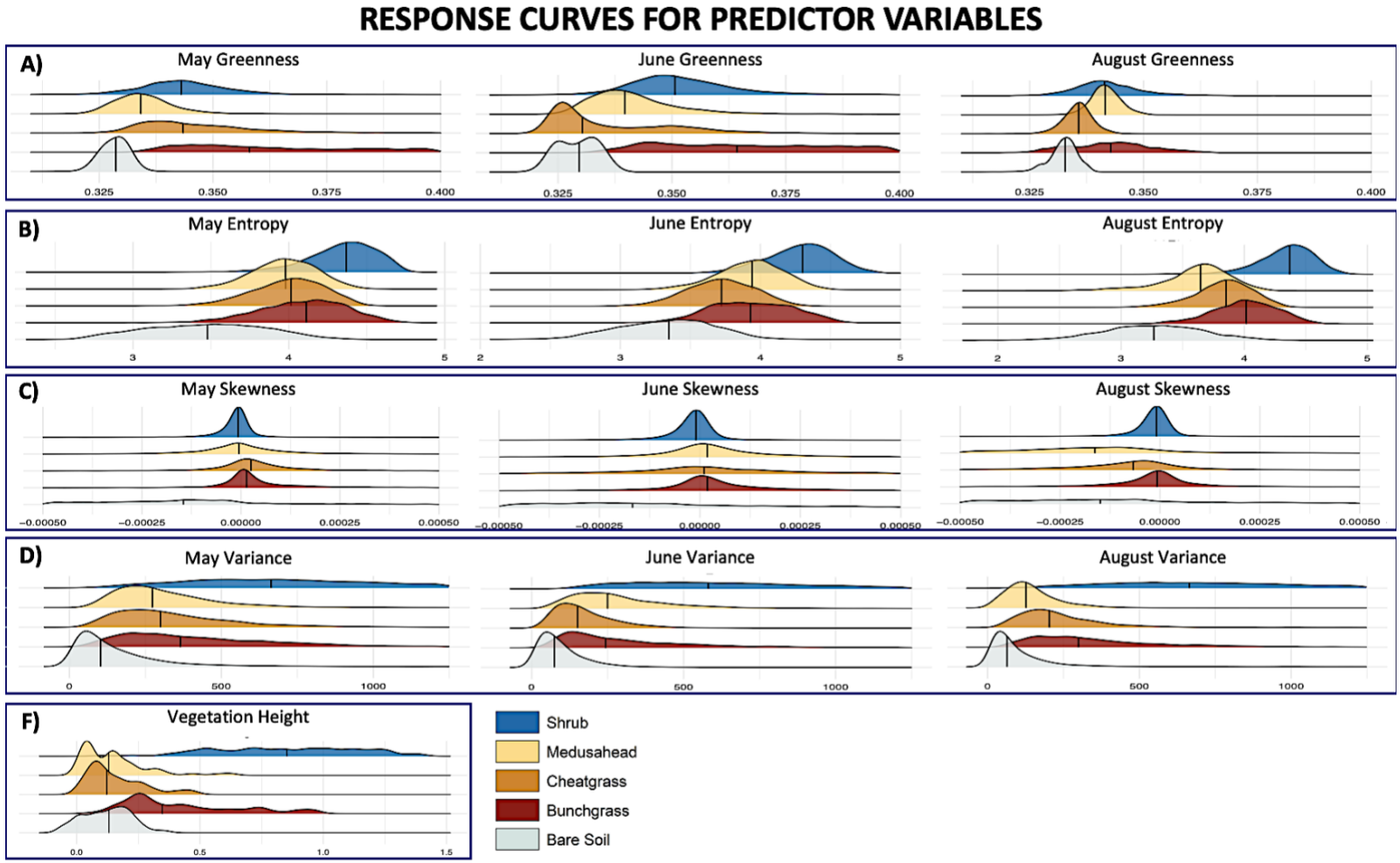

Figure 7. (A) Distributions of greenness ratio (Green Band/(Red Band + Green Band + Blue Band)) associated with class types in May, June, and August. (B) Distributions of May, June, and August entropy for each class type. (C) Distributions of May, June, and August skewness for each class type. (D) Distributions of May, June, and August variance for each class type. (E) Distributions of vegetation height for each class type.

Variability in the distributions for textural variables (entropy, skewness, and variance) separated vegetation class types on a spectrum of fine to coarse textures (Figure 7B, 7C, and 7D, and Supplementary Table 2). Of all five class types, bare soil exhibited relatively unchanged median texture values across May, June, and August, due to the homogenous nature of bare ground and rock spectral reflectance. Sagebrush and bunchgrass exhibited high median entropy (Sagebrush: May = 4.368, June= 4.301, August = 4.369, Bunchgrass: May= 4.113, June=3.930, August=4.016) and variance (Sagebrush: May = 787.490, June = 660.900, August = 778.270, Bunchgrass: May = 382.300, June = 246.610, August = 301.200) due to a greater complexity of pixel values caused by the inherent mixture of photosynthetic, non-photosynthetic, and shadow pixels these vegetation types contain within the kernel window. Shrub and bunchgrass types typically exhibited intermediate skewness (Sagebrush: May = $-7.610 \cdot 10^{-6}$, June = $-1.010 \cdot 10^{-5}$, August = $-8.512 \cdot 10^{-6}$, Bunchgrass: May = $1.510 \cdot 10^{-5}$, June = $2.274 \cdot 10^{-5}$, August = $-8.342 \cdot 10^{-6}$), where spectral values within the neighborhood kernel were as likely to be above as below the mean.

As with greenness, texture values for cheatgrass and medusahead differed from one another and co-existing vegetation over the course of the growing season (Figure 7B, 7C, and 7D, and Supplementary Table 2). Texture values for medusahead gradually became more fine, as seedlings emerged from the characteristic thatch layer of the previous year's litter. Median entropy (May = 3.979, June = 3.941, August = 3.646) and variance (May = 272.690, June = 249.670, August = 126.963) decreased slightly over the growing season, indicating greater homogeneity and uniformity of texture as medusahead stayed green

later in the season. However, entropy (May =4.014, June = 3.721, August = 3.852) and variance (May =300.220, June = 150.600, August = 203.730) for cheatgrass were more varied due to spatial variability in phenology as cheatgrass reached senescence. Both invasive grasses of interest exhibited higher negative skewness in August (Medusahead = $-2.430 \cdot 10^{-4}$, Cheatgrass = $-7.649 \cdot 10^{-5}$) when compared to bunchgrass ($-8.342 \cdot 10^{-6}$) and sagebrush ($-8.512 \cdot 10^{-6}$), suggesting large areas of relatively uniform reflectance with scattered small patches of other cover types. Cheatgrass exhibited more intermediate skewness compared to medusahead, likely due to the smaller patches of cheatgrass versus the extensive medusahead monocultures present in our study landscape.

Distributions of vegetation height further distinguished the five classes, in particular serving to distinguish the two perennial types (shrubs and perennial bunchgrasses) from the two annual grass species (cheatgrass and medusahead) (Figure 7F). Shrub species exhibited the widest range of height values (1.469), with bunchgrass second (0.992). A diversity of height values within these classes is expected because of the spectrum of species that shrub class types (e.g. sagebrush, bitterbrush) and bunchgrass class types (e.g. crested wheatgrass, squirreltail) include. Median heights for cheatgrass (0.122) and medusahead (0.130) were similar, though the range in height for cheatgrass (0.512) was slightly lower than medusahead (0.649). This pattern may be explained by the denser and taller thatch layer that medusahead creates, while cheatgrass does not exhibit the same characteristic.

Comparison Among Sites

Individual classifications using all predictor variables for each of the five study sites showed overall accuracies ranging from 0.696-0.934 (Table 4). All sites predicted cheatgrass and medusahead with reasonable or high balanced accuracy, ranging between 0.502-0.925. The PV5 site was predicted with the highest overall accuracy of 0.934 and Kappa Coefficient of 0.875. Sites PV1 and PV2 displayed overall accuracies near 0.840. The PV6 site displayed the lowest overall accuracy at 0.696, though site PV3 displayed the lowest Kappa at 0.460.

Table 4. Overall accuracies, Kappa statistics, cheatgrass balanced accuracy, and medusahead balanced accuracy for PV1, PV2, PV3, PV5, and PV6 individual-site classifications. Training data consisted of randomly sampled points within pure patches of photo-interpreted vegetation. Validation data was derived from majority vegetation. cover from 1-m^2 quadrat frames.

Site	Overall Accuracy	Kappa	Cheatgrass	Medusahead
PV1	0.860	0.655	N/A	0.916
PV2	0.826	0.668	0.502	0.850
PV3	0.736	0.460	N/A	0.833
PV5	0.934	0.875	0.925	0.912
PV6	0.696	0.576	0.845	0.734

Iterative site exclusions resulted in overall accuracies ranging between 0.670-0.758 (Table 5). Excluding site PV1 increased all statistical metrics, however overall accuracy only increased 0.061 versus using all study sites. When site PV2 was excluded from the classification, model performance declined. Exclusions of sites PV4, PV5, and PV6 were comparable to the classification using all five sites.

Table 5. Overall accuracies, Kappa statistics, cheatgrass balanced accuracy, and medusahead balanced accuracy for differing combinations of study site exclusions. Training data consisted of randomly sampled points within pure patches of photo-interpreted vegetation. Validation data was derived from majority vegetation cover from 1-m^2 quadrat frames.

Site	Overall Accuracy	Kappa	Cheatgrass	Medusahead
Using All Sites	0.745	0.611	0.765	0.834
Excluding PV1	0.806	0.707	0.805	0.897
Excluding PV2	0.670	0.509	0.755	0.791
Excluding PV3	0.745	0.614	0.785	0.796
Excluding PV5	0.750	0.6158	0.726	0.820
Excluding PV6	0.758	0.614	0.747	0.844

Model Comparisons and Selection of Predictors

Based upon the combined model across five study sites, a comparison of all 31 possible combinations of spectra, texture, and height demonstrated that the top performing multitemporal model uses information from phenology-based spectra, entropy and

skewness texture, and vegetation height variables to classify invasive annual grasses to the species level (Overall Accuracy = 0.747, Kappa = 0.613, Cheatgrass = 0.763, Medusahead = 0.833) (Table 6). However, this model is only slightly more predictive than remaining models that incorporate some combination of spectra, texture, and vegetation height. The difference in the overall accuracy for the top six models are of near identical predictive power, therefore the top model with fewer variables was more parsimonious.

Table 6. Model comparisons ranked by overall accuracy and Cohen's kappa for all study sites combined. Training data consisted of photo-interpreted patches of vegetation. Validation data consisted of vegetation field data. The top six models are highlighted in grey.

	Experiment	Overall		Cheatgrass	Medusahead
		Accuracy	Kappa	Accuracy	Accuracy
1	**RGB All Dates + Entropy + Skewness + Height**	**0.747**	**0.613**	**0.763**	**0.833**
2	RGB All Dates + Entropy + Skewness + Variance + Height	0.745	0.611	0.765	0.834
3	RGB All Dates + Entropy + Variance + Height	0.742	0.608	0.767	0.830
4	RGB All Dates + Skewness + Variance + Height	0.742	0.606	0.762	0.830
5	RGB All Dates + Variance + Height	0.742	0.606	0.766	0.827
6	RGB All Dates + Entropy + Height	0.739	0.602	0.757	0.829
7	RGB All Dates + Entropy + Skewness	0.732	0.589	0.762	0.807
8	RGB All Dates + Skewness + Height	0.730	0.586	0.738	0.819
9	RGB All Dates + Skewness + Variance	0.726	0.582	0.761	0.801
10	RGB All Dates + Entropy + Skewness + Variance	0.725	0.579	0.757	0.803
11	RGB All Dates + Entropy	0.720	0.574	0.754	0.800
12	RGB All Dates + Entropy + Variance	0.717	0.570	0.755	0.800
13	RGB All Dates + Variance	0.717	0.570	0.753	0.794

14	RGB All Dates + Height	0.716	0.567	0.732	0.814
15	RGB All Dates + Skewness	0.708	0.554	0.748	0.780
16	RGB Only, All Dates	0.682	0.515	0.729	0.763
17	Entropy + Skewness + Height	0.512	0.294	0.520	0.704
18	Entropy + Skewness + Variance + Height	0.504	0.284	0.515	0.700
19	Skewness + Variance + Height	0.500	0.281	0.5112	0.701
20	Entropy + Variance + Height	0.492	0.267	0.514	0.697
21	Skewness + Height	0.487	0.268	0.498	0.699
22	Skewness + Variance	0.4847	0.253	0.57764	0.639
23	Entropy + Skewness + Variance	0.483	0.251	0.581	0.637
24	Entropy + Skewness	0.481	0.248	0.575	0.634
25	Entropy + Height	0.475	0.252	0.494	0.693
26	Entropy Only	0.464	0.224	0.564	0.614
27	Entropy + Variance	0.462	0.225	0.569	0.619
28	Variance + Height	0.453	0.231	0.499	0.685
29	Variance Only	0.440	0.201	0.549	0.602
30	Skewness Only	0.438	0.194	0.530	0.609
31	Height Only	0.376	0.162	0.479	0.606

The phenology-based spectral variables (three RGB band ratios over three dates) contributed the most to our overall classification. When comparing the RGB, entropy, variance, skewness, and height only models, the RGB only model (model 22) resulted in the best performing model with an overall accuracy of 0.682 and Kappa of 0.515. The addition of one or several textural and height variables further increased the predictive power of the classification when added to RGB spectral bands (models 1-15). When any combination of RGB, texture, and height variables are all three incorporated into the classification (models 1-6, 8), the model always performed better than any RGB and

texture model (models 9-13, 15) or RGB and height model (model 14), with the exception of model 7. The top six best performing models included both texture and height variables in addition to the multi-temporal RGB band ratios.

To further validate our model results, RF models incorporating the same 31 combinations of spectral, textural, and vegetation height variables were also applied to photo-interpreted vegetation data for which digitized polygons (patches of vegetation) were randomly portioned into training and validation data (Supplementary Table 3). The RGB only model performed the best (Overall Accuracy = 0.901, Kappa =0.896) compared to the entropy, variance, skewness, and height only models. Any additive combination of RGB, textural, height variables increased overall model performance within 0.030. The top seven best performing models similarly exhibited at least some combination of RGB, texture, and/or height variables. While improvement was lower, the accuracy rankings of our classification as assessed using independent photo-interpreted validation data parallels that of our validation using field data from quadrat frames, confirming the predictive power of our model.

Final Model Validation

Using training data of photo-interpreted vegetation and validation data of field data taken from GPS-located quadrat frames, the best ranking model aggregated to the 2cm scale resulted in higher accuracy across all metrics. Balanced accuracy for the two invasive annual grasses of interest included cheatgrass at 0.931 and medusahead at 0.833 (Table 7). Cheatgrass and medusahead were predicted at high sensitivity (true positives;

Cheatgrass = 0.915, Medusahead = 0.942) and high specificity (true negatives; Cheatgrass = 0.947, Medusahead = 0.958). The bunchgrass and bare soil types were slightly underpredicted, while shrubs were slightly overpredicted. When cheatgrass and medusahead were misclassified, the two annual grass species were generally confused with one another more than with bare, bunchgrass, and shrub types (0.614 of cheatgrass misclassifications were classified as medusahead, 0.822 of medusahead misclassifications were classified as cheatgrass). Given that training and validation data were collected across multiple and distinct locations within our study area, these results illustrate the high generalizability of our model within the Paradise Valley landscape.

Table 7. Confusion matrix for the Random Forest classification model using all spectral, textural, and vegetation height variables (i.e. full model). Actual values of field-mapped classes are represented as columns and model-predicted classes as rows. Values along the diagonal are correct predictions, values below the diagonal are false negatives, and values above the diagonal are false positives. The table includes accuracy statistics such as sensitivity (the proportion of true positives correctly identified), specificity (the proportion of true negatives correctly identified), and balanced accuracy ([sensitivity + specificity] / 2) for each of the five vegetation class types.

Class	Reference Data					
	Bare Soil	Bunchgrass	Cheatgrass	Medusahead	Shrub	Row Total
Bare Soil	97	0	15	7	5	124
Bunchgrass	0	207	18	8	7	240
Cheatgrass	14	42	1344	102	8	1510
Medusahead	8	8	88	1954	3	2061
Shrub	6	11	4	3	658	682
Column Total	125	268	1469	2074	681	**Overall Accuracy: 0.923** **Kappa: 0.885**
Sensitivity (true positives)	0.776	0.772	0.915	0.942	0.966	
Specificity (true negatives)	0.994	0.992	0.947	0.958	0.994	
Balanced Accuracy	0.885	0.882	0.931	0.950	0.980	

Contributions of Predictors to Classification of Vegetation Types

Using mean decrease accuracy (MDA), the normalized variable importance for the top model using all spectral, entropy, skewness, and height variables indicated that the sum of phenology-based RGB spectral data was most important for class discrimination (MDA = 0.609) (Figure 8). The sum of texture variables also greatly contributed to class discrimination (MDA = 0.522). Vegetation height contributed to class discrimination the least (MDA = 0.072).

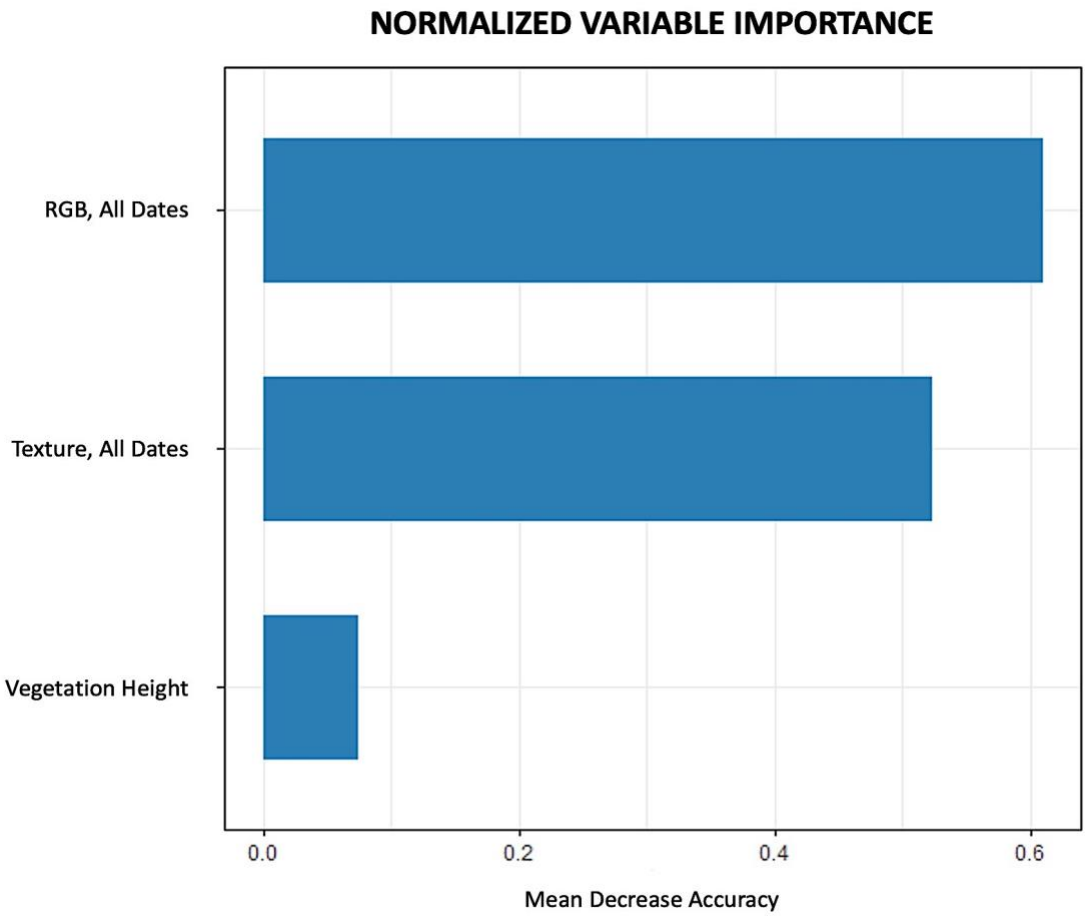

Figure 8: Variable importance plot (calculated by mean decrease accuracy) for summed predictor variables in the RF classification using all spectral, textural and vegetation height data. Variables are listed in decreasing importance.

Final Classification Map Identifying Invasive Annual Grasses to the Species Level

The random forest model containing spectral, textural, and vegetation height information successfully differentiated the two invasive annual grasses from one another and from co-occurring vegetation (Figure 9). Comparing ground truth data with the classification map shows that patches of cheatgrass, displayed in a golden-brown color, were differentiated well from the matrix of medusahead. There was some confounding of medusahead and bare soil, likely due to the bare soil spectra reflectance being similar to medusahead litter. Individual sagebrush shrubs were separated from one another, with minimal salt-and-pepper effects within shrub canopies. Shadows caused by other landscape features, such as dense thatch, were sometimes incorrectly classified as bunchgrass.

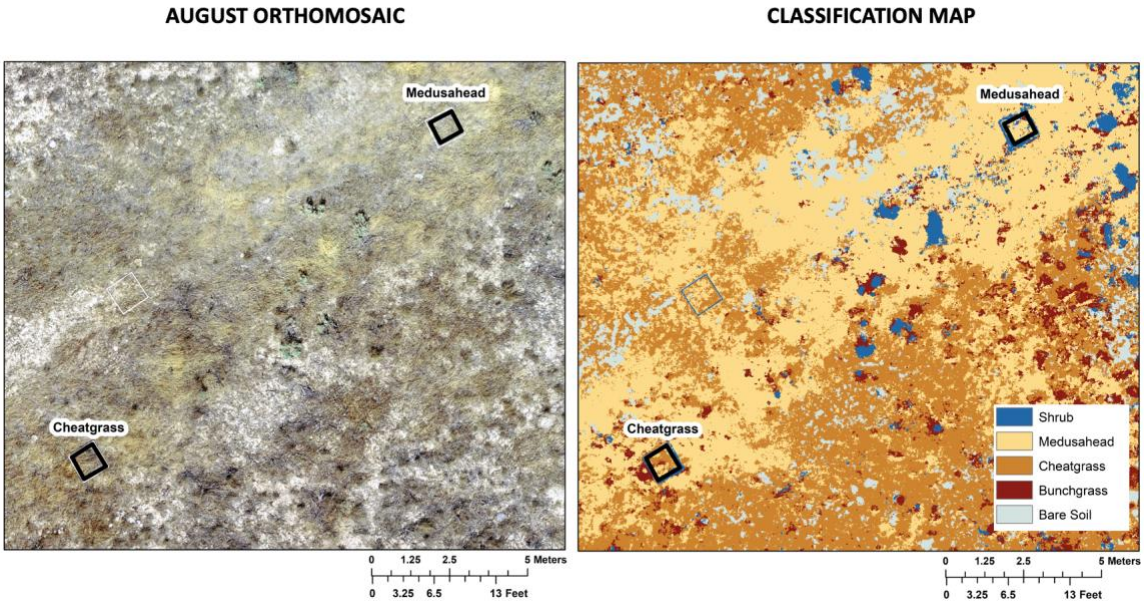

Figure 9. August UAV orthomosaic for site PV6 pictured left, featuring three vegetation quadrat frame samples. Final classification map for bare, bunchgrass, cheatgrass, bunchgrass, and sagebrush class types is pictured right. The final model utilized spectral, textural, and vegetation height data.

DISCUSSION

Our research demonstrates that the combination of multi-date textural information and photogrammetrically estimated vegetation height successfully improves a multi-temporal classification of invasive plant species. This improvement could arise from the hierarchical structure of tree-based models inherent in the RF approach. For example, vegetation height readily separates taller vegetation (shrub, bunchgrass) from shorter vegetation and bare ground (Figure 7E). Once these types have been separated, the texture variables can effectively distinguish shrub from bunchgrass, and cheatgrass or medusahead from bare ground (Figure 7B, 7C, 7D). Our methodology proved to be generalizable across multiple large rangeland landscapes containing a variety of native and invasive species.

Our invasive annual grass species of interest were predicted with high accuracy using the top-ranking model. Cheatgrass was predicted with 0.931 balanced accuracy, while medusahead was predicted at 0.950 balanced accuracy. When these species were misclassified, they generally were confused with one another versus the other vegetation types. Cheatgrass was slightly overpredicted and medusahead was slightly underpredicted in our classification. An overprediction (fewer false negatives, but more false positives) is preferred if the goals are to locate all cheatgrass patches regardless of cost and effort (Jiménez-Valverde et al., 2011), but at the expense of spending time and resources visiting sites that may not contain cheatgrass. An underprediction (fewer false positives, but more false negatives) may be preferred if the goal is to capture most medusahead

sites and there is significant cost to visiting incorrectly classified medusahead sites (Jiménez-Valverde et al., 2011).

Challenges for Remote Sensing of Invasive Plants to the Species Level

Phenological variation within and between plant species remains a notable challenge for mapping invasive plants to the species level. Previous studies have demonstrated that invasive plants can be separated from co-occurring vegetation, due to differences in the spectral characteristics of phenology during the growing season (Carson et al., 1995; Everitt et al., 1992; Peterson, 2005; Schriever and Congalton, 1995; Singh et al., 2018). In the Western United States, both Boyte et al. (2019) and Peterson et al. (2005) quantified percentage of annual grass groundcover, focusing on cheatgrass, by using several dates of imagery depicting normalized difference vegetation index (NDVI) of early spring green-up and early summer senescence. However, these approaches were challenged with separating cheatgrass from vegetation of similar phenology. For example, in Peterson et al. (2005) the estimated percent cover of cheatgrass also contained species of an invasive annual mustard (*Lepidium perfoliatum*) and a native perennial grass (*Poa secunda*) which had similar phenological characteristics to cheatgrass, thus resulting in overestimations of cheatgrass cover.

Other studies have capitalized on the plant-specific response of inter-annual rainfall to separate cheatgrass from co-occurring vegetation in the Great Basin (Bradley and Mustard, 2005; Bradley and Mustard, 2006; Balch et al., 2013). In a high rainfall year, annual grasses such as cheatgrass grows taller and establish in greater density, and

subsequentially exhibit higher greenness than in a low rainfall year. Meanwhile, shrub and perennial bunchgrasses exhibit less change in productivity due to adaptation for variance in rainfall. This approach allows mapping of cheatgrass invasions over large spatial extents, but repeatability is limited by time series data requiring both dry and wet years and selecting optimal Landsat scenes within the narrow window of peak cheatgrass productivity. While these classification techniques generate useful predictions of population patterns and percent cover, they are not species-specific and often result in aggregations of functional vegetation types (such as "early-season annuals") having broadly similar phenological characteristics (Bradley, 2014).

An additional challenge in using high-resolution mapping of invasive vegetation involves excessive detail caused by shadows and canopy gaps in vegetation. While there has been success using readily deployable, high spatial resolution imagery (such as UAV imagery) to get to the species level (Weisberg et al., 2021), purely pixel-based approaches can be less effective at high spatial resolutions and often result in misclassification and inaccuracy (de Jong et al., 2001; Kelly, et al., 2004). Consistent with the results of previous studies (Blaschke et al., 2000; Dell'Acqua and Gamba, 2006; Yoon et al., 2005), we found that inclusion of textural and height characteristics used in combination with the multitemporal spectral characteristics of a pixel improved the predictive skill of our classification (Overall Accuracy = 0.747, Kappa = 0.613, Cheatgrass = 0.763, Medusahead = 0.833 using RGB, entropy, skewness, and height vs. Overall Accuracy = 0.682, Kappa = 0.515, Cheatgrass = 0.729, Medusahead = 0.763 using RGB only). Where entirely pixel-based models often result in spectral confusion of vegetation types in

classifications utilizing high-resolution data such as UAV imagery, spatial variation in texture has previously been shown to improve the separability between class types (Feng et al., 2015). For instance, in Wisconsin marshes where cattails (*Typha spp*.) invade in high density monocultures, Boers and Zedler (2008) used the unique texture of cattails exhibiting dark circular features distinct from surrounding vegetation to map invasion rate over time. In addition, the inclusion of vegetation height derived from UAV data has been shown to increase the robustness of vegetation models (Fraser et al., 2016; van Iersel et al., 2018). While our study used single-date imagery of peak vegetation height data, van Iersel et al., (2018) used multi-date UAV imagery to derive temporal greenness as well as temporal vegetation height as a proxy for plant phenology in non-woody floodplain vegetation monitoring. Because invasive annual grasses typically emerge prior to native vegetation, this framework could potentially be applied in arid and semi-arid landscapes, such as our study region, to further the utility of vegetation height in a species-specific classification.

Caveats and Limitations of our Approach

Spatial variability in phenology is a remaining challenge for our species-specific classification approach, in which environmental variation and biological events can impact fine-scale variation in species phenology and thus the generalizability of phenology-based classifications (Andrew and Ustin, 2009; Weisberg et al., 2021). Particularly in arid and semi-arid ecosystems, pulses of plant emergence, growth, and reproductivity are directly linked to sporadic interannual rainfall (Chesson et al., 2004).

Unfortunately, accounting for inter-annual and intra-annual spatial variability in phenology for a given landscape and year is difficult to obtain prior to data collection.

Land-based digital cameras, or PhenoCams, offer a potential solution to this problem by providing high-frequency or continuous high-resolution data quantifying phenological variation, such as leaf flushing and senescence (Alberton et al., 2017; Klosterman et al. 2014; Richardson et al., 2009). This approach is ideal for observing phenological differences due to its low cost, low effort, easy installation, and ability to monitor simultaneous sites at high frequencies (e.g., hourly, daily) (Alberton et al., 2014).

Often with little consideration for how texture may vary over the growing season, texture analysis most commonly utilizes single-date imagery. Few studies have exploited variations in the phenology of texture for image classification (e.g. Culbert et al., 2009). One such study, Almeida et al. (2014), found that high levels of variation in image texture, associated with fine-scale temporal variation in vegetation greenness , were useful in characterizing deciduous (*A. tomentosum)* and evergreen (*M. rubiginosa)* species from one another. Incorporating the phenology of texture improved our ability to classify invasive annual grasses to the species level and partially mitigated the problem of interannual and spatial variability in plant phenology. Because we used the same dates of imagery for spectral and textural data, future research is needed to identify specific times during the growing season when texture measures best separate species of interest.

While our study investigated two fixed window sizes for all texture variables, several studies have suggested multi-scale methods for optimizing structural data in landscape classifications (De Siqueira et al., 2013; Lan and Liu, 2018; Marceau et al., 1990). This approach allows for differing scales, shapes, and orientations of geometric window sizes, to better account for variation in landscape features (Franklin et al., 1996; Woodcock and Strahler, 1987). For instance, at high resolutions invasive grasses may exhibit optimal window sizes at fine scales, while an optimal window for sagebrush may require coarser scales. Rather than using a single window size, further investigation of appropriate textural information at varying scales could improve our multitemporal approach.

Though occurrence texture measures mitigate misclassifications within a moving kernel, our UAV-based classification is challenged by translating across scales from patches of vegetation to individual plants. Our approach uses photo-interpreted vegetation data at the patch scale, but extracts spectral, textural, and height-based structural information at the 1cm pixel-level, resulting in occasional misclassification of pixels within vegetation patches. Such problems of high-resolution "noise" could be alleviated using an object-based image analysis (OBIA) approach, which partitions images into homogenous "image-objects" prior to classification (Blaschke, 2010; Chabot et al., 2016; Huang et al, 2020). OBIA methods differ from traditional pixel-based classifiers by segmenting defined parameters and combining neighboring pixels of similar shape, spatial, spectral, textural, contextual, and temporal data into a spatial image object (Hay et al., 2002; Ma et al., 2015; Ryherd and Woodcock, 1996). Thus, intra-class spectral variability caused by canopy gaps, shadows, and texture can be reduced by using OBIA techniques,

particularly in high-resolution images (Torres-Sánchez et al., 2015). OBIA has been used in various remote sensing applications including forest mapping, rangeland monitoring, urban mapping, and precision agriculture (de Castro et al. 2020; Feng et al. 2015; Honkavaara et al., 2013; Lu et al., 2010; Wallace et al., 2012; Weisberg et al., 2007). This technique could be an especially useful addition to our classification approach as OBIA functions at an appropriate scale relative to vegetation (Booth et al., 2005; Marceau and Hay, 1999). Ecologically meaningful features can be derived from these delineated objects, thus furthering our understanding of ecological processes and changes in the spatial pattern of vegetation (Hay et al., 2002).

Potential Applications for Resource Management and Ecological Restoration

Our methodology can further target control efforts according to the density, size, and composition of invasive vegetation. With repetitive sampling, our species-level classification allows for the early detection of new invasions (e.g. Ishii and Washitani, 2013). Because cost and effort are most feasible with the smaller scale of new invasions versus large, established infestations, the subsequent the rate of invasion is slowed while rangeland biodiversity is promoted (Baena et al., 2017; Panetta, 2009). Furthermore, historical records of invasive spread provide a useful tool for assessing the effectiveness of introduced weed management and control (Morin et al., 2009). Henderson (1999) suggests that control effectiveness can be determined at landscape scales by comparing invasive distribution in historical maps before and after the implementation of a weed control program. The change and rate of invasion over time can be evaluated with this approach, allowing for the further prioritization of control efforts and resources.

Our presence-absence data of invasive species occurrence could be integrated with bioclimatic variables for species distribution modeling (SDM) (Piiroinen et al., 2018). Across Western sagebrush ecosystems, Pastick et al. (2021) quantified historical (1985-2019), present (2020), and future (2025-2040) percent cover of invasive annual grasses with the use of field and remotely sensed data in relation to environmental variables (i.e. climate, topography, wildfire, transportation vectors). SDMs were generated from the probability of past state transitions, rate of change, and potential drivers of invasive grasses, allowing estimation of susceptibility to invasion over large areas. Because SDMs can identify suitable habitats and predict areas at high risk for future invasion, this approach provides a powerful tool for conservation, planning, and prioritized management efforts (Ahmed et al., 2020). In fact, predictions derived from SDMs have impacted global policy strategies and development in organizations such as United Nations Environment Programme, the Convention of Biological Diversity, Organization for Economic Co-operation and Development, European Union, Conservation International, International Union for Conservation of Nature, World Wildlife Fund, and more (Cayuela et al. 2009). This application is particularly relevant considering future climate change scenarios and modified disturbance regimes, in which invasive annual grasses are expected to expand into previously uninvaded areas, while at the same time, native sagebrush ecosystems are becoming less resistant to invasion (Boyte et al., 2016; Chambers et al., 2014; Chambers and Pellant, 2008; Pastick et al., 2021).

Expanding our multitemporal, phenology-based, UAV classification to satellite imagery would provide the opportunity to facilitate further management actions by capturing the general distribution of weeds over the entirety of a region rather than within a single site or several sites (Martin et al., 2018). Satellite imagery contains data over wide ranges but typically covers a mixture of vegetation types due to meter-level resolution. Contrarily, UAV imagery provides centimeter-level detail and greater flexibility in temporal resolutions but at the cost of covering smaller landscapes. Several studies have successfully combined these two modes of remote sensing to map invasive plants (Gränzig et al. 2021; Kattenborn et al. 2019). In mapping invasive shrubs (*Ulex europaeus*), Gränzig et al. (2021) successfully used UAV-based reference data to train a large-scale classification of Sentinel-2 data using optimal phenological times where *Ulex europaeus* exhibited distinct flowering phenology compared to co-existing vegetation. Over the extent of the Chiloé Island in south-central Chile, Kattenborn et al. (2019) combined UAV with multitemporal Sentinel-1 and Sentinel-2 imagery to classify three invasive plant species (*Acacia dealbata, Pinus radiata, and Ulex europaeus*) depending on intraspecific variability in canopy structure, texture, and the flowering stage. In a similar application, our results could serve as a basis for scaling to satellite-level classifications, allowing for large-scale monitoring and broad scale maps of plant invasion patterns.

Conclusion

We demonstrated the usefulness of a multitemporal classification that exploits differences in growing-season phenology, texture, and vegetation height derived from UAV imagery to classify invasive plants to the species level. Despite several caveats and inherent limitations of our methodology, our model resulted in a robust classification and offers exciting opportunity for future directions and applications. Early detection of new invasions and control effectiveness monitoring is possible with repetitive sampling and through incorporating historical imagery with our approach. Additionally, previous studies have demonstrated success in scaling detailed vegetation classifications derived from UAV imagery to satellite imagery, attaining comprehensive monitoring at regional and continental levels (Gränzig et al., 2021; Kattenborn et al., 2019). Future phenological research is needed for large-scale, species-specific modeling to facilitate resource management, targeted ecological restoration, and improved understanding of invaded ecosystems.

REFERENCES

Abatzoglou, J. T., and Kolden, C. A. (2011). Climate change in western US deserts: potential for increased wildfire and invasive annual grasses. Rangeland Ecology and Management, 64(5), 471-478.

Ahmed, N., Atzberger, C., and Zewdie, W. (2020). Integration of remote sensing and bioclimatic data for prediction of invasive species distribution in data-poor regions: a review on challenges and opportunities. Environmental Systems Research, 9(1), 1-18.

Akar, Ö., and Güngör, O. (2012). Classification of multispectral images using Random Forest algorithm. Journal of Geodesy and Geoinformation, 1(2), 105-112.

Alberton, B., Almeida, J., Helm, R., Torres, R. D. S., Menzel, A., and Morellato, L. P. C. (2014). Using phenological cameras to track the green up in a cerrado savanna and its on-the-ground validation. Ecological Informatics, 19, 62-70.

Alberton, B., Torres, R. D. S., Cancian, L. F., Borges, B. D., Almeida, J., Mariano, G. C., dos Santos, J. and Morellato, L. P. C. (2017). Introducing digital cameras to monitor plant phenology in the tropics: applications for conservation. Perspectives in Ecology and Conservation, 15(2), 82-90.

Almeida, J., dos Santos, J. A., Alberton, B., Torres, R. D. S., and Morellato, L. P. C. (2014). Applying machine learning based on multiscale classifiers to detect remote phenology patterns in cerrado savanna trees. Ecological Informatics, 23, 49-61.

Andrew, M. E., and Ustin, S. L. (2009). Effects of microtopography and hydrology on phenology of an invasive herb. Ecography, 32(5), 860-870.

Archer, S. R., and Predick, K. I. (2008). Climate change and ecosystems of the southwestern United States. Rangelands, 30(3), 23-28.

Baena, S., Moat, J., Whaley, O., and Boyd, D. S. (2017). Identifying species from the air: UAVs and the very high resolution challenge for plant conservation. PloS One, 12(11), e0188714.

Balch, J. K., Bradley, B. A., D'Antonio, C. M., and Gómez-Dans, J. (2013). Introduced annual grass increases regional fire activity across the arid western USA (1980–2009). Global Change Biology, 19(1), 173-183.

Blaschke, T. (2010). Object based image analysis for remote sensing. ISPRS Journal of Photogrammetry and Remote Sensing, 65(1), 2-16.

Blaschke, T., Lang, S., Lorup, E., Strobl, J., and Zeil, P. (2000). Object-oriented image processing in an integrated GIS/remote sensing environment and perspectives for

environmental applications. Environmental Information for Planning, Politics and the Public, 2, 555-570.

Boers, A. M., and Zedler, J. B. (2008). Stabilized water levels and *Typha* invasiveness. Wetlands, 28(3), 676-685.

Booth, D. T., Cox, S. E., Fifield, C., Phillips, M., and Williamson, N. (2005). Image analysis compared with other methods for measuring ground cover. Arid Land Research and Management, 19(2), 91-100.

Boyte, S. P., Wylie, B. K., and Major, D. J. (2016). Cheatgrass percent cover change: comparing recent estimates to climate change-driven predictions in the northern Great Basin. Rangeland Ecology and Management, 69(4), 265-279.

Boyte, S. P., Wylie, B. K., and Major, D. J. (2019). Validating a time series of annual grass percent cover in the sagebrush ecosystem. Rangeland Ecology and Management, 72(2), 347-359.

Bradley, B. A. (2014). Remote detection of invasive plants: a review of spectral, textural and phenological approaches. Biological Invasions, 16(7), 1411-1425.

Bradley, B. A., and Mustard, J. F. (2005). Identifying land cover variability distinct from land cover change: cheatgrass in the Great Basin. Remote Sensing of Environment, 94(2), 204-213.

Bradley, B. A., and Mustard, J. F. (2006). Characterizing the landscape dynamics of an invasive plant and risk of invasion using remote sensing. Ecological Applications, 16(3), 1132-1147.

Bradley, B. A., Houghton, R. A., Mustard, J. F., and Hamburg, S. P. (2006). Invasive grass reduces aboveground carbon stocks in shrublands of the Western US. Global Change Biology, 12(10), 1815-1822.

Breiman, L., Cutler, A., Liaw, A., and Wiener, M (2018). randomForest: Breiman and Cutler's Random Forests for Classification and Regression. R package version 4.6-14. https: //cran.r-project.org/web/packages/randomForest/

Brooks, M. L., D'Antonio, C. M., Richardson, D. M., Grace, J. B., Keeley, J. E., DiTomaso, J. M., Hobbs, R. J., Pellant, M. and Pyke, D. (2004). Effects of invasive alien plants on fire regimes. BioScience 54(7), 677-688.

Carson, H. W., Lass, L. W., and Callihan, R. H. (1995). Detection of yellow hawkweed (*Hieracium pratense*) with high resolution multispectral digital imagery. Weed Technology, 9(3), 477-483.

Cayuela, L., Golicher, D. J., Newton, A. C., Kolb, M., De Alburquerque, F. S., Arets, E. J. M. M., Alkemade, J. R. M. and Pérez, A. M. (2009). Species distribution modeling in the tropics: problems, potentialities, and the role of biological data for effective species conservation. Tropical Conservation Science, 2(3), 319-352.

Chabot, D., Dillon, C., Ahmed, O., and Shemrock, A. (2016). Object-based analysis of UAS imagery to map emergent and submerged invasive aquatic vegetation: a case study. Journal of Unmanned Vehicle Systems, 5(1), 27-33.

Chambers, J. C., Bradley, B. A., Brown, C. S., D'Antonio, C., Germino, M. J., Grace, J. B., Hardegree, S. P., Miller, R. F. and Pyke, D. A. (2014). Resilience to stress and disturbance, and resistance to *Bromus tectorum* L. invasion in cold desert shrublands of western North America. Ecosystems, 17(2), 360-375.

Chambers, J. C., and Pellant, M. (2008). Climate change impacts on northwestern and intermountain United States rangelands. Rangelands, 30(3), 29-33.

Chesson, P., Gebauer, R. L., Schwinning, S., Huntly, N., Wiegand, K., Ernest, M. S., Sher, A., Novoplansky, A. and Weltzin, J. F. (2004). Resource pulses, species interactions, and diversity maintenance in arid and semi-arid environments. Oecologia, 141(2), 236-253.

Coburn, C. A., and Roberts, A. C. (2004). A multiscale texture analysis procedure for improved forest stand classification. International Journal of Remote Sensing, 25(20), 4287-4308.

Culbert, P. D., Pidgeon, A. M., Louis, V. S., Bash, D., and Radeloff, V. C. (2009). The impact of phenological variation on texture measures of remotely sensed imagery. IEEE Journal of Selected Topics in Applied Earth Observations and Remote Sensing, 2(4), 299-309.

Curran, P. (1980). Multispectral remote sensing of vegetation amount. Progress in Physical Geography, 4(3), 315-341.

Cutler, D. R., Edwards Jr, T. C., Beard, K. H., Cutler, A., Hess, K. T., Gibson, J., and Lawler, J. J. (2007). Random forests for classification in ecology. Ecology, 88(11), 2783-2792.

D'Antonio, C. M., and Vitousek, P. M. (1992). Biological invasions by exotic grasses, the grass/fire cycle, and global change. Annual Review of Ecology and Systematics, 23(1), 63-87.

Davies, K. W., and Johnson, D. D. (2008). Managing medusahead in the Intermountain West is at a critical threshold. Rangelands, 30(4), 13-15.

Davies, K. W., and Sheley, R. L. (2007). Influence of neighboring vegetation height on seed dispersal: implications for invasive plant management. Weed Science, 55(6), 626-630.

de Castro, A. I., Peña, J. M., Torres-Sánchez, J., Jiménez-Brenes, F. M., Valencia-Gredilla, F., Recasens, J., and López-Granados, F. (2020). Mapping *Cynodon dactylon* infesting cover crops with an automatic decision tree-OBIA procedure and UAV imagery for precision viticulture. Remote Sensing, 12(1), 56.

de Jong, S. M., Hornstra, T., and Maas, H. G. (2001). An integrated spatial and spectral approach to the classification of Mediterranean land cover types: the SSC method. International Journal of Applied Earth Observation and Geoinformation, 3(2), 176-183.

Dell'Acqua, F., and Gamba, P. (2006). Discriminating urban environments using multiscale texture and multiple SAR images. International Journal of Remote Sensing, 27(18), 3797-3812.

de Sá, N. C., Castro, P., Carvalho, S., Marchante, E., López-Núñez, F. A., and Marchante, H. (2018). Mapping the flowering of an invasive plant using unmanned aerial vehicles: is there potential for biocontrol monitoring? Frontiers in Plant Science, 9, 293.

de Siqueira, F. R., Schwartz, W. R., and Pedrini, H. (2013). Multi-scale gray level co-occurrence matrices for texture description. Neurocomputing, 120, 336-345.

Doody, T. M., Lewis, M., Benyon, R. G., and Byrne, G. (2014). A method to map riparian exotic vegetation (*Salix* spp.) area to inform water resource management. Hydrological Processes, 28(11), 3809-3823.

Everitt, J. H., Alaniz, M. A., Escobar, D. E., and Davis, M. R. (1992). Using remote sensing to distinguish common (*Isocoma coronopifolia*) and Drummond goldenweed (*Isocoma drummondii*). Weed Science, 40(4), 621-628.

Feng, Q., Liu, J., and Gong, J. (2015). UAV remote sensing for urban vegetation mapping using random forest and texture analysis. Remote Sensing, 7(1), 1074-1094.

Ferro, C. J. and Warner, T. A., 2002. Scale and texture in digital image classification. Photogrammetric Engineering and Remote Sensing, 68(1), 51-63.

Franklin, S. E., Wulder, M. A., and Lavigne, M. B. (1996). Automated derivation of geographic window sizes for use in remote sensing digital image texture analysis. Computers and Geosciences, 22(6), 665-673.

Fraser, R. H., Olthof, I., Lantz, T. C., and Schmitt, C. (2016). UAV photogrammetry for mapping vegetation in the low-Arctic. Arctic Science, 2(3), 79-102.

Ge, S., Carruthers, R., Gong, P., and Herrera, A. (2006). Texture analysis for mapping *Tamarix parviflora* using aerial photographs along the Cache Creek, California. Environmental Monitoring and Assessment, 114(1), 65-83.

Gränzig, T., Fassnacht, F. E., Kleinschmit, B., and Förster, M. (2021). Mapping the fractional coverage of the invasive shrub *Ulex europaeus* with multi-temporal Sentinel-2 imagery utilizing UAV orthoimages and a new spatial optimization approach. International Journal of Applied Earth Observation and Geoinformation, 96, 102281.

Griffith, G. E., Omernik, J. M., Smith, D. W., Cook, T. D., Tallyn, E. D., Moseley, K., and Johnson, C. B. (2016). Ecoregions of California. US Geological Survey Open-File Report, 1021.

Hall-Beyer, M. (2000). GLCM Texture: A Tutorial. National Council on Geographic Information and Analysis Remote Sensing Core Curriculum, 3, 75.

Haralick, R. M., and Shanmugam, K. S. (1974). Combined spectral and spatial processing of ERTS imagery data. Remote Sensing of Environment, 3(1), 3-13.

Haralick, R. M., Shanmugam, K., and Dinstein, I. H. (1973). Textural features for image classification. IEEE Transactions on Systems, Man, and Cybernetics, 6, 610-621.

Hay, G. J., Dubé, P., Bouchard, A., and Marceau, D. J. (2002). A scale-space primer for exploring and quantifying complex landscapes. Ecological Modelling, 153(1-2), 27-49.

Henderson, L. (1999). The Southern African Plant Invaders Atlas (SAPIA) and its contribution to biological weed control. African Entomology, 1, 159-163.

Heywood, V. H. (1989). Patterns, extents and modes of invasions by terrestrial plants. Biological invasions: a global perspective, 31-60.

Hironaka, M. (1994). Medusahead: natural successor to the cheatgrass type in the northern Great Basin. Proceedings: Ecology and Management of Annual Rangelands. USDA Forest Service General Technical Report INT-GTR-313, 89-91.

Huang, C. Y., and Asner, G. P. (2009). Applications of remote sensing to alien invasive plant studies. Sensors, 9(6), 4869-4889.

Huang, H., Lan, Y., Yang, A., Zhang, Y., Wen, S., and Deng, J. (2020). Deep learning versus Object-based Image Analysis (OBIA) in weed mapping of UAV imagery. International Journal of Remote Sensing, 41(9), 3446-3479.

Honkavaara, E., Saari, H., Kaivosoja, J., Pölönen, I., Hakala, T., Litkey, P., Mäkynen, J. and Pesonen, L. (2013). Processing and assessment of spectrometric, stereoscopic imagery collected using a lightweight UAV spectral camera for precision agriculture. Remote Sensing, 5(10), 5006-5039.

Hulbert, L. C. (1955). Ecological studies of *Bromus tectorum* and other annual bromegrasses. Ecological Monographs, 25(2), 181-213.

Irons, J. R., and Petersen, G. W. (1981). Texture transforms of remote sensing data. Remote Sensing of Environment, 11, 359-370.

Ishii, J., and Washitani, I. (2013). Early detection of the invasive alien plant *Solidago altissima* in moist tall grassland using hyperspectral imagery. International Journal of Remote Sensing, 34(16), 5926-5936.

Ji, W., and Wang, L. (2016). Phenology-guided saltcedar (*Tamarix* spp.) mapping using Landsat TM images in western US. Remote Sensing of Environment, 173, 29-38.

Jiménez-Valverde, A., Peterson, A. T., Soberón, J., Overton, J. M., Aragón, P., and Lobo, J. M. (2011). Use of niche models in invasive species risk assessments. Biological Invasions, 13(12), 2785-2797.

Joshi, C., De Leeuw, J., and van Duren, I. C. (2004). Remote sensing and GIS applications for mapping and spatial modelling of invasive species. In Proceedings of ISPRS (Vol. 35, p. B7).

Justice, C. O., Townshend, J. R. G., Holben, B. N., and Tucker, E. C. (1985). Analysis of the phenology of global vegetation using meteorological satellite data. International Journal of Remote Sensing, 6(8), 1271-1318.

Kattenborn, T., Lopatin, J., Förster, M., Braun, A. C., and Fassnacht, F. E. (2019). UAV data as alternative to field sampling to map woody invasive species based on combined Sentinel-1 and Sentinel-2 data. Remote Sensing of Environment, 227, 61-73.

Kelly, M., Shaari, D., Guo, Q., and Liu, D. (2004). A comparison of standard and hybrid classifier methods for mapping hardwood mortality in areas affected by sudden oak death. Photogrammetric Engineering and Remote Sensing, 70(11), 1229-1239.

Kerr, J. T., and Ostrovsky, M. (2003). From space to species: ecological applications for remote sensing. Trends in Ecology and Evolution, 18(6), 299-305.

Klosterman, S.T., Hufkens, K., Gray, J.M., Melaas, E., Sonnentag, O., Lavine, I., Mitchell, L., Norman, R., Friedl, M.A. and Richardson, A.D. (2014). Evaluating remote

sensing of deciduous forest phenology at multiple spatial scales using PhenoCam imagery. Biogeosciences, 11(16), 4305-4320.

Kumar, S., Melkani, N., Awasthi, N., and Prakash, R. (2015). Texture analysis and classification of polarimetric SAR images using histogram measures. In 2015 2nd International Conference on Signal Processing and Integrated Networks (SPIN) (pp. 506-511). IEEE.

Laliberte, A. S., and Rango, A. (2009). Texture and scale in object-based analysis of subdecimeter resolution unmanned aerial vehicle (UAV) imagery. IEEE Transactions on Geoscience and Remote Sensing, 47(3), 761-770.

Lan, Z., and Liu, Y. (2018). Study on multi-scale window determination for GLCM texture description in high-resolution remote sensing image geo-analysis supported by GIS and domain knowledge. ISPRS International Journal of Geo-Information, 7(5), 175.

Lu, D., Hetrick, S., and Moran, E. (2010). Land cover classification in a complex urban-rural landscape with QuickBird imagery. Photogrammetric Engineering and Remote Sensing, 76(10), 1159-1168.

Lawrence, R. L., Wood, S. D., and Sheley, R. L. (2006). Mapping invasive plants using hyperspectral imagery and Breiman Cutler classifications (RandomForest). Remote Sensing of Environment, 100(3), 356-362.

Ma, L., Cheng, L., Li, M., Liu, Y., and Ma, X. (2015). Training set size, scale, and features in Geographic Object-Based Image Analysis of very high resolution unmanned aerial vehicle imagery. ISPRS Journal of Photogrammetry and Remote Sensing, 102, 14-27.

Mack, R. N., Simberloff, D., Mark Lonsdale, W., Evans, H., Clout, M., and Bazzaz, F. A. (2000). Biotic invasions: causes, epidemiology, global consequences, and control. Ecological Applications, 10(3), 689-710.

Marceau, D. J., and Hay, G. J. (1999). Contributions of remote sensing to the scale issues. Canadian Journal of Remote Sensing, 25(4), 357-366.

Marceau, D. J., Howarth, P. J., Dubois, J. M. M., and Gratton, D. J. (1990). Evaluation of the grey-level co-occurrence matrix method for land-cover classification using SPOT imagery. IEEE Transactions on Geoscience and Remote Sensing, 28(4), 513-519.

Martin, F. M., Müllerová, J., Borgniet, L., Dommanget, F., Breton, V., and Evette, A. (2018). Using single-and multi-date UAV and satellite imagery to accurately monitor invasive knotweed species. Remote Sensing, 10(10), 1662.

Marushia, R. G., Cadotte, M. W., and Holt, J. S. (2010). Phenology as a basis for management of exotic annual plants in desert invasions. Journal of Applied Ecology, 47(6), 1290-1299.

Melgoza, G., Nowak, R. S., and Tausch, R. J. (1990). Soil water exploitation after fire: competition between *Bromus tectorum* (cheatgrass) and two native species. Oecologia 83(1), 7-13.

Morin, L., Reid, A. M., Sims-Chilton, N. M., Buckley, Y. M., Dhileepan, K., Hastwell, G. T., Nordblom, T. L. and Raghu, S. (2009). Review of approaches to evaluate the effectiveness of weed biological control agents. Biological Control, 51(1), 1-15.

Nafus, A. M., and Davies, K. W. (2014). Medusahead ecology and management: California annual grasslands to the Intermountain West. Invasive Plant Science and Management, 7(2), 210-221.

Ndzeidze, S. K. (2011). Detecting medusahead (*Taeniatherum caput-medusae*) using high frequency, sequential, globally positioned digital images. Ph.D. thesis, Oregon State University, Corvallis, OR.

Panetta, F. D. (2009). Weed eradication—an economic perspective. Invasive Plant Science and Management, 2(4), 360-368

Pastick, N. J., Wylie, B. K., Rigge, M. B., Dahal, D., Boyte, S. P., Jones, M. O., Allred, B. W., Parajuli, S. and Wu, Z. (2021). Rapid monitoring of the abundance and spread of exotic annual grasses in the western United States using remote sensing and machine learning. AGU Advances, 2(2), e2020AV000298.

Peterson, E. B. (2005). Estimating cover of an invasive grass (*Bromus tectorum*) using tobit regression and phenology derived from two dates of Landsat ETM+ data. International Journal of Remote Sensing, 26(12), 2491-2507.

Piiroinen, R., Fassnacht, F. E., Heiskanen, J., Maeda, E., Mack, B., and Pellikka, P. (2018). Invasive tree species detection in the Eastern Arc Mountains biodiversity hotspot using one class classification. Remote Sensing of Environment, 218, 119-131.

Räsänen, A., and Virtanen, T. (2019). Data and resolution requirements in mapping vegetation in spatially heterogeneous landscapes. Remote Sensing of Environment, 230, 111207.

Reed, B. C., Brown, J. F., VanderZee, D., Loveland, T. R., Merchant, J. W., and Ohlen, D. O. (1994). Measuring phenological variability from satellite imagery. Journal of Vegetation Science, 5(5), 703-714.

Richardson, A. D., Braswell, B. H., Hollinger, D. Y., Jenkins, J. P., and Ollinger, S. V. (2009). Near-surface remote sensing of spatial and temporal variation in canopy phenology. Ecological Applications, 19(6), 1417-1428.

Riou, R., and Seyler, F. (1997). Texture analysis of tropical rain forest infrared satellite images. Photogrammetric Engineering and Remote Sensing, 63(5), 515-521.

Rosso, P. H., Ustin, S. L., and Hastings, A. (2006). Use of lidar to study changes associated with *Spartina* invasion in San Francisco Bay marshes. Remote Sensing of Environment, 100(3), 295-306.

Ryherd, S., and Woodcock, C. (1996). Combining spectral and texture data in the segmentation of remotely sensed images. Photogrammetric Engineering and Remote Sensing, 62(2), 181-194.

Schriever, J. R., and Congalton, R. G. (1995). Evaluating seasonal variability as an aid to cover-type mapping from Landsat Thematic Mapper data in the Northeast. Photogrammetric Engineering and Remote Sensing, 61(3), 321-327.

Shannon, C. E. (1948). A mathematical theory of communication. The Bell System Technical Journal, 27(3), 379-423.

Singh, K. K., Chen, Y. H., Smart, L., Gray, J., and Meentemeyer, R. K. (2018). Intra-annual phenology for detecting understory plant invasion in urban forests. ISPRS Journal of Photogrammetry and Remote Sensing, 142, 151-161.

Straatsma, M. W., and Baptist, M. J. (2008). Floodplain roughness parameterization using airborne laser scanning and spectral remote sensing. Remote Sensing of Environment, 112(3), 1062-1080.

Sutherland, W. J. (2006). Predicting the ecological consequences of environmental change: a review of the methods. Journal of Applied Ecology, 43(4), 599-616.

Torres-Sánchez, J., López-Granados, F., and Peña, J. M. (2015). An automatic object-based method for optimal thresholding in UAV images: Application for vegetation detection in herbaceous crops. Computers and Electronics in Agriculture, 114, 43-52.

Tortorelli, C. M., Krawchuk, M. A., and Kerns, B. K. (2020). Expanding the invasion footprint: *Ventenata dubia* and relationships to wildfire, environment, and plant communities in the Blue Mountains of the Inland Northwest, USA. Applied Vegetation Science, 23(4), 562-574.

Unser, M. (1986). Local linear transforms for texture measurements. Signal Processing, 11(1), 61-79.

Van de Voorde, T., De Genst, W., and Canters, F. (2007). Improving pixel-based VHR land-cover classifications of urban areas with post-classification techniques. Photogrammetric Engineering and Remote Sensing, 73(9), 1017.

van Iersel, W., Straatsma, M., Addink, E., and Middelkoop, H. (2018). Monitoring height and greenness of non-woody floodplain vegetation with UAV time series. ISPRS Journal of Photogrammetry and Remote Sensing, 141, 112-123.

Wallace, L., Lucieer, A., Watson, C., and Turner, D. (2012). Development of a UAV-LiDAR system with application to forest inventory. Remote Sensing, 4(6), 1519-1543.

Walker, B., and Steffen, W. (1997). An overview of the implications of global change for natural and managed terrestrial ecosystems. Conservation Ecology, 1(2).

Weidner, U., and Förstner, W. (1995). Towards automatic building extraction from high-resolution digital elevation models. ISPRS journal of Photogrammetry and Remote Sensing, 50(4), 38-49.

Weisberg, P. J., Dilts, T. E., Greenberg, J. A., Johnson, K. N., Pai, H., Sladek, C., Kratt, C., Tyler, S. W. and Ready, A. (2021). Phenology-based classification of invasive annual grasses to the species level. Remote Sensing of Environment, 263, 112568.

Weisberg, P. J., Lingua, E., and Pillai, R. B. (2007). Spatial patterns of pinyon–juniper woodland expansion in central Nevada. Rangeland Ecology and Management, 60(2), 115-124.

Westoby, M. J., Brasington, J., Glasser, N. F., Hambrey, M. J., and Reynolds, J. M. (2012). 'Structure-from-Motion' photogrammetry: A low-cost, effective tool for geoscience applications. Geomorphology, 179, 300-314.

Whittingham, C. P. (1974). The mechanisms of photosynthesis. London: Edward Arnold.

Wood, E. M., Pidgeon, A. M., Radeloff, V. C., and Keuler, N. S. (2012). Image texture as a remotely sensed measure of vegetation structure. Remote Sensing of Environment, 121, 516-526.

Woodcock, C. E., and Strahler, A. H. (1987). The factor of scale in remote sensing. Remote sensing of Environment, 21(3), 311-332.

Xu, C., Holmgren, M., Van Nes, E. H., Maestre, F. T., Soliveres, S., Berdugo, M., Kéfi, S., Marquet, P. A., Abades, S. and Scheffer, M. (2015). Can we infer plant facilitation from remote sensing? A test across global drylands. Ecological Applications, 25(6), 1456-1462.

Yoon, G. W., Cho, S. I., Chae, G. J., and Park, J. H. (2005). Automatic land-cover classification of Landsat images using feature database in a network. In Proceedings of the IGARSS 2005 symposium, Seoul, Korea.

Young, J. A. (1992). Ecology and management of medusahead (*Taeniatherum caput-medusae* ssp. *asperum* [Simk.] Melderis). The Great Basin Naturalist, 245-252.

Young, J. A., and Longland, W. S. (1996). Impact of alien plants on Grant Basin rangelands. Weed Technology, 10(2), 384-391.

SUPPLEMENTARY MATERIALS

Post-classification aggregation comparisons

While the 1cm scale classification was used to train the RF model, predictions were aggregated based on the majority pixel values for model validation. We found the 2cm scale classification to perform the best out of multiple resamples, with an overall accuracy of 87% and a Cohen's Kappa Coefficient of 80% (Supplementary Table 1). Accuracy in cheatgrass predictions improved from being underpredicted at the 1cm scale to being slightly overpredicted at the 2cm scale.

Supplementary Table 1. Comparison of overall accuracies using all spectral, textural, and height-based data for each aggregated scale.

Scale	Overall Accuracy	Kappa	Cheatgrass	Medusahead
1cm	0.747	0.613	0.763	0.833
2cm	0.923	0.885	0.931	0.950
3cm	0.917	0.876	0.927	0.944
5cm	0.882	0.823	0.895	0.921

Statistics for Exploratory Data Analysis

Supplementary Table 2. Median (Minimum, Maximum) values over the growing season for predictor variables of photo-interpreted vegetation types used as training data. Vegetation height was only calculated for June, during peak height.

		MAY	JUNE	AUGUST
GREENNESS	Bare	0.329 (0.309, 0.338)	0.330 (0.310, 0.341)	0.312 (0.312,0.339)
	Bunchgrass	0.377 (0.332, 0.690)	0.378 (0.325, 0.636)	0.343 (0.303, 0.379)
	Cheatgrass	0.344 (0.310, 0.479)	0.330 (0.318, 0.419)	0.336 (0.316, 0.349)
	Medusahead	0.334 (0.316, 0.377)	0.340 (0.321, 0.411)	0.342 (0.328, 0.356)
	Sagebrush	0.343 (0.000, 0.500)	0.351 (0.294, 0.720)	0.346 (0.290, 0.500)
ENTROPY	Bare	3.477 (2.506,4.445)	3.346 (2.201, 4.299)	3.265 (1.843, 4.419)
	Bunchgrass	4.113 (2.996, 4.782)	3.930 (2.697, 4.672)	4.016 (2.978, 4.740)
	Cheatgrass	4.014 (3.069, 4.558)	3.721 (2.863, 4.445)	3.852 (2.829, 4.459)
	Medusahead	3.979 (3.195, 4.724)	3.941 (2.914, 4.587)	3.646 (2.311, 4.344)
	Sagebrush	4.368 (2.441, 4.823)	4.301 (3.346, 4.870)	4.369 (3.201, 4.916)
SKEWNESS	Bare	$-3.027 \cdot 10^{-4}$ $(-2.611 \cdot 10^{-2}, 2.526 \cdot 10^{-2})$	$-7.876 \cdot 10^{-4}$ $(-5.790 \cdot 10^{-2}, 4.201 \cdot 10^{-4})$	$-7.876 \cdot 10^{-2}$ $(-2.080 \cdot 10^{-1}, 4.313 \cdot 10^{-2})$
	Bunchgrass	$1.510 \cdot 10^{-5}$ $(-1.355 \cdot 10^{-3}, 2.334 \cdot 10^{-3})$	$2.274 \cdot 10^{-5}$ $(-7.235 \cdot 10^{-3}, 5.532 \cdot 10^{-3})$	$-8.342 \cdot 10^{-6}$ $(-2.472 \cdot 10^{-3}, 1.889 \cdot 10^{-2})$
	Cheatgrass	$2.748 \cdot 10^{-5}$ $(-1.399 \cdot 10^{-3}, 4.150 \cdot 10^{-3})$	$2.191 \cdot 10^{-5}$ $(-3.441 \cdot 10^{-3}, 6.733 \cdot 10^{-3})$	$-7.649 \cdot 10^{-5}$ $(-4.381 \cdot 10^{-3}, 3.760 \cdot 10^{-3})$
	Medusahead	$-4.093 \cdot 10^{-6}$ $(-1.812 \cdot 10^{-3}, 2.049 \cdot 10^{-3})$	$2.196 \cdot 10^{-5}$ $(-2.545 \cdot 10^{-3}, 4.958 \cdot 10^{-3})$	$-2.430 \cdot 10^{-4}$ $(-4.471 \cdot 10^{-2}, 2.944 \cdot 10^{-2})$
	Sagebrush	$-7.610 \cdot 10^{-6}$ $(-2.001 \cdot 10^{-3}, 3.362 \cdot 10^{-2})$	$-1.010 \cdot 10^{-5}$ $(-1.847 \cdot 10^{-3}, 1.130 \cdot 10^{-3})$	$-8.512 \cdot 10^{-6}$ $(-1.231 \cdot 10^{-3}, 1.344 \cdot 10^{-3})$
VARIANCE	Bare	103.180 (10.180, 1471.590)	74.784 (5.524, 856.360)	64.177 (2.522, 1211.850)
	Bunchgrass	382.300 (27.850, 2552.910)	246.610 (15.410, 1840.15)	301.200 (26.920, 2529.370)
	Cheatgrass	300.220 (33.430, 1541.040)	150.600 (21.800, 1193.300)	203.730 (19.410, 1184.460)

	Medusahead	272.690 (41.610, 2112.320)	249.670 (22.470, 1353.440)	126.963 (6.561, 846.273)
	Sagebrush	787.490 (12.540, 3401.270)	660.900 (70.100, 5654.100)	778.270 (42.680, 5012.830)
VEGETATION HEIGHT	Bare	0.131 (-0.069, 0.376)		
	Bunchgrass	0.348 (0.029, 1.021)		
	Cheatgrass	0.122 (-0.009, 0.503)		
	Medusahead	0.130 (-0.004, 0.645)		
	Sagebrush	0.859 (-0.036, 1.433)		

Model verification using only photo-interpreted vegetation data

Photo-interpreted polygons of vegetation data were randomly split into 50% training and 50% validation data. All additive combinations of spectral, textural, and vegetation height variables were applied to the RF model using photo-interpreted polygons only (Supplementary Table 3). The top model resulted in an overall accuracy of 0.929, Kappa of 0.906, and balanced accuracies of cheatgrass at 0.906 and medusahead at 0.946. Accuracy statistics and model combinations generally follow the same pattern as compared to models using photo-interpreted data for training and quadrat frame data for validation, indicating a robust model. This model verification further strengthens the interpretation that texture and vegetation height information improved our classification.

Supplementary Table 3. Overall models ranked by overall accuracy and Cohen's kappa using PV1, PV2, PV3, and PV6. Training and validation data consists of randomly partitioned photo-interpreted patches of vegetation. The top five models are highlighted in grey.

	Experiment	Overall		Cheatgrass	Medusahead
		Accuracy	Kappa	Accuracy	Accuracy
1	**RGB All Dates + Entropy + Skewness**	**0.929**	**0.906**	**0.906**	**0.946**
2	RGB All Dates + Skewness + Variance	0.928	0.905	0.903	0.946
3	RGB All Dates + Entropy + Skewness + Variance	0.927	0.904	0.905	0.944
4	RGB All Dates + Entropy + Skewness + Variance + Height	0.927	0.903	0.903	0.945
5	RGB All Dates + Entropy + Variance	0.926	0.903	0.901	0.943
6	RGB All Dates + Entropy + Skewness + Height	0.925	0.900	0.894	0.947
7	RGB All Dates + Skewness + Variance + Height	0.924	0.900	0.893	0.947
8	RGB All Dates + Entropy	0.924	0.900	0.899	0.944
9	RGB All Dates + Variance	0.923	0.898	0.893	0.946

10	RGB All Dates + Entropy + Variance + Height	0.923	0.898	0.896	0.944
11	RGB All Dates + Entropy + Height	0.922	0.897	0.890	0.946
12	RGB All Dates + Variance + Height	0.922	0.897	0.890	0.945
13	RGB All Dates + Skewness + Height	0.920	0.894	0.881	0.949
14	RGB All Dates + Skewness	0.916	0.889	0.884	0.940
15	RGB All Dates + Height	0.908	0.878	0.863	0.940
16	RGB Only	0.901	0.869	0.863	0.930
17	Skewness + Variance + Height	0.738	0.656	0.735	0.785
18	Entropy + Skewness + Variance + Height	0.737	0.655	0.736	0.786
19	Entropy + Skewness + Height	0.734	0.651	0.727	0.783
20	Entropy + Variance + Height	0.701	0.609	0.710	0.775
21	Skewness + Height	0.690	0.595	0.680	0.745
22	Entropy + Skewness	0.688	0.589	0.700	0.773
23	Skewness + Variance	0.688	0.589	0.708	0.774
24	Entropy + Skewness + Variance	0.686	0.587	0.702	0.775
25	Entropy + Height	0.676	0.578	0.671	0.764
26	Variance + Height	0.668	0.567	0.667	0.762
27	Entropy + Variance	0.638	0.525	0.680	0.750
28	Entropy Only	0.632	0.516	0.667	0.743
29	Skewness Only	0.620	0.502	0.662	0.709
30	Variance Only	0.611	0.491	0.666	0.732
31	Height Only	0.464	0.310	0.560	0.603